REVIEW

How to go beyond C$_1$ products with electrochemical reduction of CO$_2$

Da Li,[†ab] Hao Zhang,[†a] Hang Xiang,[b] Shahid Rasul,[c] Jean-Marie Fontmorin,[bh] Paniz Izadi,[bi] Alberto Roldan, [ID][d] Rebecca Taylor, [ID][e] Yujie Feng, [ID][f] Liam Banerji,[g] Alexander Cowan, [ID] *[g] Eileen Hao Yu [ID] *[abf] and Jin Xuan [ID] *[a]

The electrochemical reduction of CO$_2$ to produce fuels and value-added organic chemicals is of great potential, providing a mechanism to convert and store renewable energy within a carbon-neutral energy circle. Currently the majority of studies report C$_1$ products such as carbon monoxide and formate as the major CO$_2$ reduction products. A particularly challenging goal within CO$_2$ electrochemical reduction is the pursuit of multi-carbon (C$_{2+}$) products which have been proposed to enable a more economically viable value chain. This review summaries recent development across electro-, photoelectro- and bioelectro-catalyst developments. It also explores the role of device design and operating conditions in enabling C−C bond generation.

1. Introduction

The concentration of CO$_2$ in the atmosphere has hit its highest level in history, reaching over 420 ppm in 2021.[1] It is widely accepted that the greenhouse effect caused by CO$_2$ accumulation is the main reason for global warming and climate change, which is threatening sustainable life on earth. Carbon Capture and Utilization (CCU) is one way to deal with the ever-increasing CO$_2$ concentration in the atmosphere. Electrochemical CO$_2$ reduction (ECO$_2$R), utilizing renewable energy resources is potentially an efficient process to convert the waste CO$_2$, captured from the atmosphere and/or industrial processes. ECO$_2$R has an added advantage in its use as "energy storage" technology, where intermittent renewable energy is utilized to store electrons in high energy density chemical bonds.[2–4] At present, ECO$_2$R conversion to C$_1$ is well established, however, there are several challenges for the ECO$_2$R process to scale-up at

industrial scale i.e. process energy efficiency, product selectivity and inaccessibility to multi-carbon (C$_{2+}$) products from the reaction. Indeed, multi-carbon (C$_{2+}$) products from ECO$_2$R are attractive from the industrial application point of view due to their higher energy density, well-established chemistry and available infrastructure for processing and transportation.[2–4]

The reduction of CO$_2$ to stable C$_{2+}$ species is extremely challenging, for example, for C$_2$ compounds such as C$_2$H$_4$ and C$_2$H$_5$OH, 12-electrons need to be transferred to the reaction centre, whilst for C$_3$ compounds such as C$_3$H$_7$OH 18 electrons are transferred.[5,6] To date two main strategies have been used to achieve C$_{2+}$ products. Firstly, the discovery and design of a single electrocatalyst able to convert CO$_2$ to C$_{2+}$ at a low overpotential has been targeted. However, the large number of proton and electron transfers required leads to complex,
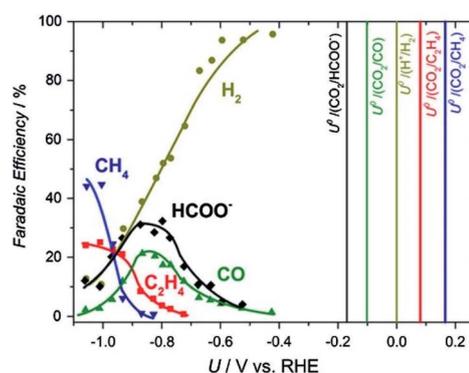
[a]Department of Chemical Engineering, Loughborough University, Loughborough, LE11 3TU, UK. E-mail: e.yu@lboro.ac.uk; J.Xuan@lboro.ac.uk

[b]School of Engineering, Newcastle University, Newcastle Upon Tyne, NE1 7RU, UK

[c]Faculty of Engineering and Environment, Northumbria University, Newcastle Upon Tyne, NE1 8ST, UK

[d]Cardiff Catalysis Institute, School of Chemistry, Cardiff University, Cardiff, CF 10 3AT, UK

[e]Department of Chemical Engineering and Analysis Science, University of Manchester, Manchester, M13 9PL, UK

[f]School of Environment, Harbin Institute of Technology, Harbin, 150090, PR China

[g]Department of Chemistry, University of Liverpool, Liverpool, L69 7ZF, UK. E-mail: A.J. Cowan@liverpool.ac.uk

[h]Univ Rennes, CNRS, ISCR, UMR 6226, 35000 Rennes, France

[i]Helmholtz Centre for Environmental Research GmbH - UFZ, Department of Environmental Microbiology, Permoserstraße 15, 04318 Leipzig, Germany

† Authors contributed to the work equally.

Fig. 1 Product faradaic efficiency (FE) vs. potential at −5 mA cm^{-2} on a Cu electrode in 0.1 M KHCO$_3$. The vertical lines show the standard thermodynamic potentials.[11] Reproduced from ref. 11 with permission from Elsevier, copyright 2016.

multiple reaction pathways being accessible and the similarity of the equilibrium potentials for many products (*e.g.* C_2H_4, C_2H_5OH, and C_3H_7OH are ~0.1 V *vs.* RHE, Fig. 1) makes the generation of a wide product distribution likely in the absence of a highly selective catalyst.[7,8] The difficulty of generating a single catalytic centre, or several centres within a single material, which have optimized binding energies for the wide-range of intermediates to be formed is clearly extremely challenging and to date this, coupled to the low aqueous solubility of CO_2, has typically led to low partial current densities and selectivities for C_{2+} production. An alternative strategy is to separate the overall reduction of CO_2 to products into two separate steps: (i) initial reduction of CO_2 electrochemically to C_1 compounds (CO), and (ii) reduction of C_1 products into C_2, C_3 and higher carbon-containing liquid fuels.[9] By focusing on the further reduction of C_1 compounds, the demands on the catalyst can be reduced with a lower number of intermediates as compared to the reduction of CO_2 as starting reactant. Furthermore, CO is found to be an intermediate[7,10] in the reduction of CO_2 to fuels and other useful chemicals, which makes this method more attractive.

From a mechanistic point of view, it is well known that during the ECO_2R, once CO_2 is activated, CO is formed on the electrode surface and the rate-determining step for the ECO_2R is a reaction involving adsorbed *CO.[11,12] Also, adsorbed intermediates such as HCOO* (ref. 7 and 13) and COOH* (ref. 14 and 15) have been identified experimentally and validated from theoretical calculations. Although computational simulations of electrochemical systems are exceptionally challenging,[16] various types of model approximations have been developed to theoretically investigate the electrode–electrolyte interface: (i) the hydrogen electrode model,[17] and (ii) the water solvated and shuttling model.[18]

Among many of the metallic electrocatalysts tested, only Cu based electrocatalysts are proven to show electrocatalytic activity for either CO_2 or CO reduction to produce hydrocarbons at reasonable FEs and oxygenates with a reasonable selectively however at the cost of a high overpotential.[19,20] This is a developing field with promising strategies revolving around Cu based structures with low coordinated active sites generated by engineered defects, tuned oxidation states and modified electronic structures with the addition of binary/ternary metallic structures.

In this review, after only briefly summarizing the state-of-the-art in the development of Cu based electrodes for the generation of C_{2+} products by ECO_2R, we focus instead on strategies beyond Cu electrode design. A summary of the current state of the art of alternative approaches to metal electrodes; such as the use molecular electrocatalysts and bio-electrochemical approaches for the synthesis of hydrocarbons from ECO_2R are reported. We then present the recent developments, and critical role, that electrochemical reactor design and electrolyte engineering (*e.g.* through the use of novel ionic liquids) can have in controlling activity towards C_{2+} production formation. Finally, the challenges and strategies of developing advanced catalysts, mechanistic understanding and reactors design are proposed to guide the future R&D of ECO_2R.

2. Electrocatalysts for C_{2+} products

2.1 Metals/metal oxide electrocatalysts

2.1.1 Cu – the incomparable role in C–C coupling. There are multiple recent review articles[21–31] that focus on the design and structuring of metallic, particularly Cu, electrodes for the production of C_{2+} hydrocarbons or oxygenates from ECO_2R. The important step for C_{2+} products is the C–C coupling, which dependences with the overpotential is still in debate but certainly it is linked to the pH.[32–35] While experimental trends and DFT results showed that C–C coupling takes place at lower potentials than CHO* hydrogenations on Cu, the entire reaction mechanisms are still under debate as experimental observations attributed the C–C formation to the Eley–Rideal mechanism between two CO species.[36,37]

Cu with the specific electron configuration in d sub-shell is able to activate CO_2 with more than two pairs of the proton-electron transfer. Of the transition metals Cu is the only elemental metal reported to catalyse ECO_2R to multi-carbon products. Research from Kuhl *et al.*[38] observed 16 types of carbonaceous products, *i.e.*, 4 C_1, 6 C_2, and 5 C_3, from ECO_2R catalysed by polycrystalline Cu in CO_2-saturated 0.1 M $KHCO_3$. Among the C_{2+} products, only C_2H_4 and C_2H_5OH produced with higher than 10% FE. Table 1 summarizes works that produce C_{2+} products from ECO_2R using heterogeneous electrocatalysts including metal (or metal-oxide) and carbon materials. Generally, C_2H_4 and C_2H_5OH have been achieved with higher selectivity than other C_{2+} products. The highest FEs reported so far are 87% (ref. 39) (C_2H_4) and 93.2% (ref. 40) (C_2H_5OH), indicating the greatest potential for further development and application. Thus, it appears promising to try to enhance the selectivity of these two valuable C_2 products by modification of Cu catalyst. This has been approached by the following four ways.

Altering the lattice/crystal structure of Cu. A facet-dependent activity for CO_2 electroreduction toward C_{2+} products has been demonstrated.[41,42] Hori *et al.*[43] in 2002 used a series of single-crystal Cu electrodes to investigate the effect of the crystal structure of the Cu electrode on ECO_2R performance. The results demonstrated the dependence of product selectivity on the Cu crystal structure: Cu(111) typically generates CH_4, while Cu(100) gives preference to C_{2+} products, often C_2H_4. These experimental results can be rationalised by the relative stability of CO on different Cu surfaces. CO dimerization is an important route to C–C bond formation[44,45] and it has been found that the formation of absorbed CO dimer occurs more easily, and is most stable, on the square arrangement of 4 surface atoms, *i.e.*, the (100) crystal plane.[46] In 2003 Hori *et al.*[47] tested a Cu electrode with a mixed crystal surface, which was Cu[4(100) × (111)] composed of 4 atomic rows of (100) terraces and one atomic height of the (111) step. It was shown to be an effective material for C_2H_4 formation (the FE reached up to 50% with a C_2H_4/CH_4 ratio around 13.5), indicating that the stepped surface mixed with (100) and (111) is more favourable for ethylene formation. Therefore, synthesis of Cu nanoparticles with high Cu(100) exposure serves as a guideline for designing a catalyst towards

Table 1 An overview of heterogeneous electrocatalysts for C_{2+} products from ECO_2R^a

Catalyst/cathode material	Applied potential (V vs. RHE)	Current density (mA cm^{-2})	Electrolyte	C$_{\geq 2}$ FEs (%)							Ref.
				C$_2$H$_4$	C$_2$H$_5$OH	C$_2$H$_6$	CH$_3$COOH	C$_3$H$_7$OH	C$_3$H$_5$OH	Other C$_{2+}$	
Altering the lattice/crystal structure of Cu Polycrystalline Cu	−1.0	5	0.1 M KHCO$_3$	30.1	6.9	N.G.	N.G.	3.0	N.G.	N.G.	51
Polycrystalline Cu	−1.05	~6.2	0.1 M KHCO$_3$	26.0	9.8	N.G.	0.3	2.3	1.1	0.28 (C$_2$H$_4$O$_2$) 0.33 (C$_2$H$_4$O) 0.12 (C$_2$H$_6$O$_2$) 0.08 (C$_3$H$_6$O)	38
Cu(100)	N.G.	5	0.1 M KHCO$_3$	40.7	12.8	N.G.	2.5	1.6	0.7	1.0 (C$_2$H$_4$O) 1.2 (C$_3$H$_6$O)	43
Cu(111)	N.G.	5	0.1 M KHCO$_3$	8.8	5.3	N.G.	1.1	<0.05	<0.05	2.6 (C$_2$H$_4$O)	43
Cu(S)-[4(100) × (111)]	N.G.	5	0.1 M KHCO$_3$	50.0	7.4	N.G.	0.9	4.6	2.2	1.2 (C$_2$H$_4$O) 5.2 (C$_3$H$_6$O)	47
Enhancing the surface roughness of Cu Cu NPs surface	−1.1	N.G.	0.1 M KClO$_4$	35.5	N.G.	<0.5	N.G.	N.G.	N.G.	N.G.	52
Electro-deposited Cu	−1.3	N.G.	0.1 M KHCO$_3$	33.3	N.G.	<0.5	N.G.	N.G.	N.G.	N.G.	53
Ex situ electro-deposited Cu	−1.3	N.G.	0.1 M KHCO$_3$	11	N.G.	2.1	N.G.	N.G.	N.G.	N.G.	54
Cu nanofoam	−1.1	N.G.	0.1 M KHCO$_3$	1.4	N.G.	1.2	N.G.	N.G.	N.G.	0.13 (C$_3$H$_6$)	55
15 nm Cu NPs	−1.1	22	0.1 M KHCO$_3$	3	N.G.	N.G.	N.G.	N.G.	N.G.	N.G.	56
Cu nano-flower	−1.3	~18	0.1 M KHCO$_3$	19	N.G.	N.G.	N.G.	N.G.	N.G.	N.G.	57
44 nm Cu nano-cube	−1.1	N.G.	0.1 M KHCO$_3$	41	4	N.G.	N.G.	3	<0.1	2 (C$_2$H$_4$O)	58
Glycine treated Cu nano-wire	−1.3	N.G.	0.1 M KHCO$_3$	12.7	N.G.	21.1	N.G.	N.G.	N.G.	0.3 (C$_3$H$_6$)	59
Cu inverse opal-6 layers	−0.81	~15	0.1 M KHCO$_3$	29.2	9.32	N.G.	0.36	3.35	N.G.	1 (C$_2$H$_2$O$_2$) 0.12 (C$_2$H$_4$O$_2$) 0.13 (C$_2$H$_6$O$_2$)	60
O$_2$ plasma-modified Cu dendrites	−0.9	~30	0.1 M KHCO$_3$	29	12	N.G.	N.G.	N.G.	N.G.	N.G.	61
Oxide-derived Cu catalysts [100] Cu$_2$O film	−1.1	N.G.	0.1 M KHCO$_3$	21.5	N.G.	1.5	N.G.	N.G.	N.G.	N.G.	62
Oxygen-evacuated Cu$_2$O	−1.2	N.G.	0.5 M KHCO$_3$	25	N.G.	N.G.	N.G.	N.G.	N.G.	N.G.	63
0.9 μm Cu$_2$O film	−0.99	25	0.1 M KHCO$_3$	40.3	8.66	0.04	N.G.	N.G.	N.G.	N.G.	64
OH-mediated Cu NPs	−0.54	225	10 M KOH	66	11	N.G.	7	N.G.	N.G.	N.G.	65
OH-mediated Cu NPs	−0.79	~300	0.5 M KHCO$_3$	45.6	17.4	N.G.	2.5	4.5	N.G.	N.G.	66
Alloying and compositing Cu with other components Au NPs covered Cu$_2$O	−1.05	28.08	0.1 M KHCO$_3$	38.7	22.6	N.G.	0.85	6.83	N.G.	1.10 (C$_2$H$_4$O)	67
Phase-blended Ag–Cu$_2$O	−1.20	~2.5	0.1 M KHCO$_3$	9.5	34.15	0.1	N.G.	N.G.	N.G.	5.65 (CH$_3$COOH + C$_2$H$_4$O)	68
Ag-saturated Cu(100) + Ag surface alloy	−1.0	N.G.	0.05 M Cs$_2$CO$_3$	42	12.5	N.G.	2	6	2.5	1 (C$_2$H$_4$O) 2.5 (C$_3$H$_6$O)	69
CuSn alloy	−0.8	225	1 M KOH	56.7	22.9	N.G.	4.7	0	N.G.	N.G.	70
Bimetallic Ag/Cu	−0.67	250	1 M KOH	35	41	N.G.	6	N.G.	N.G.	N.G.	71
N-Doped graphene supported Cu NPs	−1.2	N.G.	0.1 M KHCO$_3$	N.G.	63	N.G.	N.G.	N.G.	N.G.	N.G.	72

Table 1 (Contd.)

Catalyst/cathode material	Applied potential (V vs. RHE)	Current density (mA cm^{-2})	Electrolyte	C$_{\geq 2}$ FEs (%)							Ref.
				C$_2$H$_4$	C$_2$H$_5$OH	C$_2$H$_6$	CH$_3$COOH	C$_3$H$_7$OH	C$_3$H$_5$OH	Other C$_{2+}$	
Organics-modified Cu Pyridinic-N rich graphene supported Cu NPs (7 nm)	−0.9	N.G.	0.5 M KHCO$_3$	19	N.G.	<2	N.G.	N.G.	N.G.	N.G.	73
Cu–N–C	−1.2	16.2	0.1 M CsHCO$_3$	0	43	N.G.	N.G.	N.G.	N.G.	N.G.	74
Polycrystalline Cu with N-substituted pyridinium	−1.1	1.02	0.1 M KHCO$_3$	40.5	30.6	N.G.	N.G.	7.1	N.G.	N.G.	75
Catalysts besides Cu N-Doped nanodiamond/Si rod array	−1.0	∼6.5	0.5 M NaHCO$_3$	N.G.	N.G.	N.G.	77.6	N.G.	N.G.	N.G.	76
N-Doped mesoporous carbon	−0.56	0.5	0.1 M KHCO$_3$	N.G.	77	N.G.	N.G.	N.G.	N.G.	N.G.	77
Pd-multiwalled carbon nanotubes	4 V (cell voltage)	∼5.3	0.8 M KHCO$_3$	N.G.	N.G.	N.G.	38.7	N.G.	N.G.	N.G.	78

^{a} RHE, reversible hydrogen electrode; FEs, faradaic efficiencies; N.G., not given.

C$_{2+}$ products.[48] Cu cubes dominated by Cu(100) catalysed CO$_2$-to-C$_2$H$_4$ with a FE of 57% at a moderate potential of −0.65 V versus RHE. By contrast, Cu octahedrons with Cu(111) terraces reached a selectivity for CH$_4$.[41] Sargent et al. developed Cu(100)-rich Cu nanoparticles which showed a strong adsorption capability to intermediates, such an electrode achieved nearly 90% FE for C$_2$ products.[49] A recent calculation work demonstrated that increasing CO coverage on the Cu(111) surface decreased the C–C coupling energy, favouring to C$_2$ products, especially ethanol.[50]

Enhancing the surface roughness of Cu. Roughened Cu electrodes have a high density of exposed surface grain boundaries, such as steps, edges, and defects. These grain boundaries are commonly considered as the active sites for ECO$_2$R.[79–82] Wang et al. utilized a facile molten salt decomposition method to prepare a nanostructured Cu@Cu$_2$(OH)$_3$NO$_3$ electrode. Cu$_2$(OH)$_3$NO$_3$ is converted into metallic Cu during CO$_2$ electroreduction, leaving abundant defects on the dendritic rough surface. Benefiting from the highly rough surface, this electrode achieved a high selectivity for C$_2$H$_4$ production with a FE of 31.80%.[81] The concave octahedral Cu$_2$O catalyst with the abundant active sites derived from the in situ-generated crystal defects/grain boundaries were suggested to account for the improved C–C coupling during the ECO$_2$R.[82]

Different shapes or textures of the micro- or nano-sized Cu catalysts present different types of grain boundaries. A leaf-like CuO nanosheet fabricated on nitrogen doped graphene displayed a high-curvature structure and multiple distinguished grain boundaries to enhance the selectivity to C$_2$H$_4$ with a high FE of 30%.[83] Porous copper nanospheres with higher specific surface area and richer pores were designed. Such a porous structure greatly improved the C–C coupling process by enriching *CO intermediates in the pore structure. As a result,

a high C$_2$ selectivity with a FE of 57.22% was achieved, about 2.5-fold than the compact Cu.[84]

The plasma treated Cu foil was efficient to create a rough surface with numerous undercoordinated sites that bound CO preferentially.[85] Roughened surfaces also contained square sites with neighbouring step sites, which adsorbed the precursor *OC–COH for C$_{2+}$ products. As a result, the FE for C$_2$ products (C$_2$H$_4$ and C$_2$H$_5$OH) increased from ∼30% to 55%. More importantly, the increased roughening of the Cu surface increased the ratio of current densities for C$_{2+}$ to C$_1$ products up to a maximum value of ∼9 for a surface roughness factor of ∼3.

Oxide-derived Cu catalysts. In reality, Cu electrodes prepared by electrodeposition in aqueous solution always have an oxidized outer layer which was reported to reduce the overpotential for the formation of carbonaceous products. Therefore, there has been intense interests in the role that oxide-derived (OD) Cu may have had in achieving enhanced ECO$_2$R performance.[86–92] Similar to the metallic Cu electrode, OD-Cu generally show a wide C$_1$–C$_3$ product distribution from ECO$_2$R, but seem to be more preferable in the production of C$_{2+}$ products.[89,90] Cuprous oxide (Cu$_2$O) is widely proposed to be a more efficient OD-Cu for CH$_3$OH production, due to its moderate binding energy to methoxy (CH$_3$O*) adsorbates (key intermediates for CH$_3$OH formation).[62] Theoretical studies showed that the intermediate CH$_3$O* can transform to CH$_4$ or CH$_3$OH depending on whether the interacting surface is metallic Cu or oxidized Cu.[93] Chang et al.[94] proposed that the key factor was the availability of surface oxygen vacancies, particularly those formed by the reduction of Cu$_4$O$_3$ surface, which could stabilize the CO dimer. However it is important to note that Cu oxides can be fully reduced to metallic Cu at less-negative potential than ECO$_2$R.[64,88,95] This has led some to state that the active phase for ECO$_2$R is metallic Cu.[89,96,97] For

instance, Cu oxides were fully reduced to metallic Cu during ECO_2R, which showed even better C_{2+} selectivity compared to the untreated counterparts, suggesting the C_{2+} selectivities did not link to the specific oxidation states of Cu.[98] However, this has been disputed as some studies demonstrated the existence of subsurface oxygen of OD-Cu during ECO_2R, confirmed by ^{18}O isotope labelling,[99] in situ surface-enhanced Raman spectroscopy,[88] and in situ ambient pressure X-ray photoelectron spectroscopy.[100] The residual subsurface oxygen was proposed to enhance the binding energy and coverage of $*CO$[100] and thus raise the possibility of CO dimerization.[101] Also, a higher local pH offering a substantial amount of OH groups was assumed to facilitate the stabilization of the residual oxygen.[99,102]

Alloying and compositing Cu with other components. Alloying Cu with other metals is a widely studied approach to reduce the reaction overpotential and adjust the product distribution. Alloying modifies the surface lattice strain that affects the intermediates adsorption energies.[103,104] In addition, the second metal generates high abundance of CO which is subsequently spilled over to Cu sites that are active for the C–C coupling.[105,106] To date, reports increasingly see alloy catalysts to show better selectivity of C_{2+} from ECO_2R than Cu alone, and these all use Cu-rich alloys (or metallic composites) containing another CO-selective metal, such as Au,[107–111] Ag,[27,105,106,112–114] and Zn.[115–119] Alloying Cu with a CO producing metal is considered to deliver synergetic effects derived by the availability of C–C coupling sites (Cu) to CO-producing atoms (e.g. Au, Ag, and Zn).[120] Compared to the ~55% FE with Cu_2O electrode, C_2–C_3 with up to 65% FE were produced by using a Ag–Cu_2O bimetallic electrode, with the greatest selectivity towards C_2H_4.[113] The mechanism of improved C_2 activity was proposed to be due to the expanded Cu–Ag distances compared to metallic Cu–Cu distances, which changed the binding energies of adsorbates and intermediates, thus favouring the formation of C_{2+} products. A controlled selectivity of C_2H_5OH production from ECO_2R was achieved by varying the elemental arrangement of Ag and Cu in a Ag–Cu_2O composite.[68] More specifically, the FE of C_2H_5OH increased from 20% to 35% with the enhanced surface atomic composition of Ag from 0.12 to 0.22. A CO-insertion mechanism was hypothesised, which is briefly CO reacting with $*CH_2$ species on the Ag–Cu biphasic boundary. Phase-segregated Ag/Cu composites obtained an enhancement in the FE for C_2H_5OH by 2.3-fold and in the partial current density for CO_2 reduction by 5-fold compared with the pure Cu counterpart.[106] Results also indicated C_2H_5OH production scaled with the amount of CO evolved from Ag sites and the abundance of Cu–Ag boundaries.

Zn is also known for its high selectivity to CO, therefore CO intermediates could first be generated at its Zn sites, which would then be transferred to adjacent Cu sites for further reduction into hydrocarbon products. B-doped Cu–Zn gas diffusion electrodes exhibited excellent selectivity for C_{2+} (C_2H_4, C_2H_5OH, C_3H_7OH) with a FE value of 70% at −0.54 V vs. RHE.[118] The close proximity of Cu and Zn atoms on the surface of the catalyst was found to facilitate both stabilization of the CO$*$ intermediate and its transfer from Zn atoms to their neighboured Cu for further dimerization and protonation.[121]

Similarly, hierarchically porous Cu/Zn alloy catalysts also showed a higher selectivity towards C_2 products. The FE of C_2H_5OH reached 46.6% and the total FE of liquid C_2 products closed to 60% at −0.8 V vs. RHE. The Cu/Zn catalysts promoted the adsorption of CO_2 and simultaneously suppressed adsorption of protons. The tendency of C–C coupling could be controlled by the Zn content in Cu/Zn alloys.[117]

Non-metals as components in Cu composites also have shown an ability to promote C–C coupling from ECO_2R. Sulphur, an alternative chalcogen to oxygen, has been reported to be an efficient promoter for C_2H_5OH formation by a Cu_2S–Cu core–shell catalyst containing high levels of Cu vacancies.[122] The synergy between subsurface sulphur atoms and copper vacancy defects shifts the product preference to C_2H_5OH with suppressed C_2H_4 production. Boron-doped CuO nanobundles designed for CO_2 reduction have abundant oxygen vacancies, the increased exposure of accessible active sites and the CO_2 adsorption capacity facilitated to the C_2H_4 production with the FE of 58.4%.[123]

2.1.2 Other metal electrocatalysts besides Cu. Producing C_{2+} from ECO_2R by other metals besides Cu has been reported to exhibit excellent multi-carbon product selectivity. Significant progress has also been achieved recently for CO_2 reduction to multi-carbon products on Ag, Cr, Mo, Mn, Fe, In and Co-based electrodes.[44] Anchoring Ag nanoparticles onto 3D graphene-wrapped nitrogen-doped carbon foam was reported to efficiently and preferentially convert CO_2 to C_2H_5OH with FE of 82.1–85.2% at −0.6 to −0.7 V vs. RHE.[124] Such a high selectivity could be attributed to the synergistic effect between the pyridinic N, which exhibited a higher bonding ability toward CO$*$ intermediates, and the Ag nanoparticles that converted the CO$*$ to the $*OC$–COH intermediate of C_2H_5OH. AgCo surface alloy electrocatalysts also show a high activity for C_2H_5OH production. This high intrinsic activity is attributed to the reduced energy barrier for $*CO_2^{\delta-}$ formation as a result of the introduction of Co atoms; leading to the increased coverage of CO$*$ and C–C coupling to form $*OC$–CO$*$ on Ag atoms.[125] A 3D FeP nanoarray on Ti mesh electrode acted as an efficient catalyst electrode for the CO_2 reduction reaction to convert CO_2 into alcohols.[126] Although FE for C_2H_5OH was only 14.1%, it provided a new direction to design non-Cu catalysts for C_{2+} products. C_5 products were first produced by palladium–gold,[127] albeit at low FE's, with a hypothesized mechanism of $*CH_2$ polymerization. This seems to open a potential way to produce long carbon-chain products from ECO_2R, but the lack of detailed mechanistic studies is a significant barrier preventing further development of the approach.

2.2 Molecular catalysts

Small molecular electrocatalysts provide well defined active sites that can be synthetically tuned, offering a pathway to control the mechanisms of inner-sphere electron transfer between the catalyst and substrate that occur following initial reduction(s) of the catalyst at the electrode surface. Therefore, molecular electrocatalysts may provide access to lower over-potentials and improved selectivity towards the desired

products.[128] Indeed, turn-over frequencies in excess 10^6 per catalyst at overpotentials as low as 0.2 V have now been reported[129] for the reduction of CO_2 to CO in aprotic solvents and the field continues to develop rapidly. However, it is striking that the vast majority of studies using molecular electrocatalysts only report the formation of the simplest C_1 products (CO, HCOOH), formed by the 2-electron, 2-proton-reduction of CO_2 and progress towards these products is covered in multiple recent reviews.[128,130,131] This can be readily understood as the majority of molecular electrocatalysts for CO_2 reduction contain a single metal site, with limited coordination flexibility, preventing either accumulation or stabilization of initially reduced C_1 species to enable subsequent C–C bond formation. Despite these challenges there are examples of catalysts that achieve C–C coupling. Two recent comprehensive reviews include molecular catalysis towards >$2e^-$ products and have extensive coverage on many of the advances to date.[132,133] The highest performing of these are covered in this section. The relatively small number of C_2 producing molecular catalysts can be broadly classed into 3 categories, each of which has a distinct approach to enabling C–C bond formation; (i) those that produce oxalate, typically *via* the use of catalysts with multiple CO_2 binding sites, (ii) Ru based catalysts that stabilize reduced carbon intermediates and (iii) heterogenized molecular electrocatalysts.

Oxalate ($C_2O_4{}^{2-}$) is arguably the simplest C_2 product and its formation during the reduction of CO_2 has been reported to occur with high FEs on relatively inert metal electrodes such as Hg and Pb in aprotic solvents at very negative potentials.[128] There, the direct 1-electron reduction of CO_2 leads to the formation of $CO_2{}^{\bullet-}$ which dimerizes. Several molecular catalysts have now been reported to facilitate oxalate formation at greatly reduced overpotentials. In early works, Tanaka and colleagues described the production of oxalate using an Ir catalyst containing three metal centres in acetonitrile.[134] Infrared spectroscopy was used to follow the mechanism allowing the authors to show that in contrast to the behaviour of CO_2 on metal electrodes, free $CO_2{}^{\bullet-}$ was not formed. Instead coupling of two reduced, bound CO_2 molecules within the catalyst was proposed to occur. A common feature of many oxalate producing catalysts[134–136] is that they consist of multiple metal centres which may be envisaged to provide an advantageous mechanism for C–C bond formation. However, intriguingly experiments on both bi- and monometallic Ru complexes demonstrated that in the absence of water both could produce C_2O_4.[129–131,134–136] Despite only having a single metal centre, mechanistic studies clearly demonstrated again that free $CO_2{}^{\bullet-}$ was not formed and instead it was proposed that reversible ligand loss could occur to enable binding of a second CO_2 molecule to the same metal atom. Of particular note is a more recent report of binuclear Cu complex that was shown to produced oxalate at very low overpotentials with >96% selectivity, which remarkably could even reduce CO_2 at the concentrations found in air, as shown in Fig. 2.[135]

A series of papers from Tanaka and colleagues used Ru based polypridyl electrocatalysts for the production of a wide range of complex multicarbon products.[137–142] Early studies on the
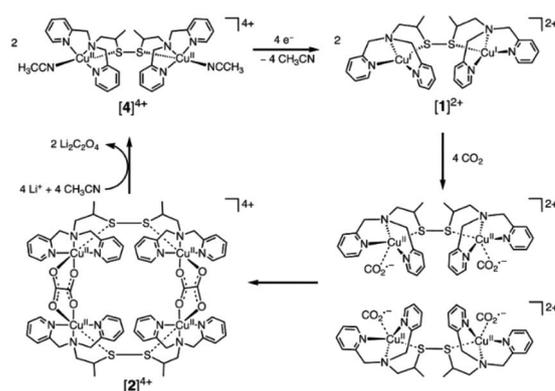

Fig. 2 Multimetallic Cu complexes have been shown to enable C–C bond formation through the coupling of multiple bound $CO_2{}^{\bullet-}$ species within the cluster giving rise to very low overpotentials and high selectivity to oxalate formation even with air as the CO_2 source.[135] Reproduced from ref. 135 with permission from American Association for the Advancement of Science, copyright 2010.

chemical, and electrochemical reduction of $[Ru(bpy)(trpy)(CO)_2]^{2+}$ in the presence of CO_2 showed marked temperature dependencies. At low temperature (-20 °C) in C_2H_5OH/H_2O mixes CO_2 electrolysis led to the formation of a range of products including formate, glycolic acid ($HOCH_2$-CO_2H) and 3-oxopropanoic acid with isotopic labelling demonstrating that both carbons were derived from CO_2.[137] In contrast, at room temperature CO and formate were the dominant products. The ability of the catalyst to generate C–C bonds at low temperature was proposed to be due to the stability of a $[Ru(bpy)(trpy)CO]^{2+}$ intermediate, allowing for further reduction and the formation of $[Ru(bpy)(trpy)(CHO)]^+$, which could then be reduced and interact with a CO_2 molecule bound at the vacant site on the Ru centre. On the other hand, at room temperature CO loss could compete preventing the formation of the key formyl intermediate.[68,142] However, it was noted that even at low temperature formate production dominated as the strong hydride donating ability of the formyl complex led to the direct reaction of CO_2 and loss of formate. Further studies by the team using naphthyridine ligands that can stabilize Ru–CO intermediates to reductive CO loss have since achieved C–C formation with high yields and selectivity even at room temperature, however, in these cases only one carbon is shown to come from CO_2 with the 2nd proposed to come from the supporting tetramethyl ammonium cation of the electrolyte *via* a methylation reaction.[138–142] Nonetheless, the approach clearly demonstrates that through careful ligand design it is possible to stabilize the initial C_1 products at a molecular catalyst to allow for C–C bond formation.

The studies of molecular catalysts described so far either use aprotic or organic/water mixes at low temperature to control the stability of key intermediates or, in the case of oxalate formation, dry solvents. However, it is widely recognised that for electrocatalytic CO_2 reduction to become viable at the scale it will need to be coupled to water oxidation, making the discovery of catalysts that can operate in aqueous conditions highly desirable.[143] Of particular interest is the reported

electrocatalytic reduction of CO_2 to form C_2 and C_3 products in aqueous electrolytes. Early studies using metal porphyrin and phthalocyanine (*e.g.* M-5,10,15,20-tetrakis-(4-methoxyphenyl) porphyrinato Co(II) and Cu(II))[144] complexes immobilised in a polymer matrix on electrode surfaces primarily yielded C_1 products but traces of C_2 products[144,145] including C_2H_6 and C_2H_4, however as will be discussed below in the following section more careful *in situ* analysis is required to confirm whether the transition metal complex is the true catalytic centre. Work by Ogura and colleagues also explored the use of polymer-coated electrodes with multiple potential catalytic centers and CO_2 binding sites for C_2–C_3 formation in water. Initial experiments with films containing both iron cyanide complexes and a cobalt co-catalyst in polyaniline (PANI) demonstrated the formation of CO_2 reduction products including C_2H_5OH and $C_3H_6O_3$, although FEs were very low (<2% for each).[146] Further studies showed that by replacing the cobalt catalyst with a 2nd iron(II) complex FEs in excess of 10% could be achieved for CO_2 reduction to $C_3H_6O_3$ at a pH of 3.[147] Subsequent mechanistic studies highlighted the important role of the PANI in CO_2 accumulation close to the catalyst centres thus enabling C–C bond formation.[148,149] It is therefore interesting to note that the majority of studies now use PTFE based polymers, which cannot facilitate such an interaction with CO_2 to aid catalyst adhesion to the electroactive support. We propose that a promising, simple avenue that should be explored by the community is the potentially beneficial role of the use of a "non-innocent" supporting polymer such as PANI.

Immobilisation of molecular catalysts onto electrodes continues to be a common factor in studies where the electrocatalytic reduction of CO_2 to C_2 occurs, however careful attention must be paid to the true nature of the active site. One study used a copper-porphyrin complex with pendant hydroxyl groups (PorCu) heterogenized on a carbon paper electrode, Fig. 3, to produce ethylene at a high partial current density (8.4 mA cm^{-2}, ~18% FE) in addition to CH_4, CO and H_2 at −0.976 V *vs.* RHE in $KHCO_3$ electrolyte.[150] The catalytic current and activity towards C_2H_4 production increased with experiment time, so a series of

Fig. 3 Electrocatalytic activity of a copper-porphyrin complex (PorCu) with pendant hydroxyl pendant hydroxyl groups heterogenized on a carbon paper electrode: (A) CV curves, (B) total current densities, (C) FE, and (D) partial current densities of gaseous products at various potentials.[150] Reproduced from ref. 150 with permission from American Chemistry Society, copyright 2016. The catalyst was later found to reversibly reconstruct into Cu nanoparticles, which provide the active site for ethylene formation.[151]

ex situ control experiments (absorption/fluorescence spectroscopy, mass spectroscopy, TEM, XPS) were performed to test the nature of the active catalyst. Whilst these found no evidence for degradation *ex situ*, a follow-up study by the same group[151] utilised *in situ* and *operando* X-ray adsorption spectroscopy (XAS) to investigate three copper based molecular catalysts for ECO_2R and noted that at −1.06 V *vs.* RHE the Cu(0) state was dominant. Extended X-ray adsorption fine structure (EXAFS) demonstrated the appearance of a bond peak at 2.2 Å, consistent with Cu–Cu bonds in metallic copper under reducing conditions. Interestingly the initial Cu(II) state was regenerated upon switching back to the open circuit potential, demonstrating reversible metal nanoparticle formation from the molecular Cu complex. As reversible nanoparticle formation has now been confirmed to occur under reducing conditions for a range of catalysts including PorCu, it seems likely that similar behavior was also occurring in the early studies where trace C_2 products were formed using Cu based molecular catalysts in polymer supports[144] and also these more recent studies. Indeed a dinuclear copper tris(2-benzimidazolylmethyl)amine (Cu$_2$(NTB)) complex which shows amongst the highest FE for C_2H_4 (42% at −1.28 V *vs.* RHE) has also been recently reported whilst also showing similar reversible Cu nanoparticle formation, with the metallic nanoparticle the likely active catalyst.[152]

There is evidence that both reversible and irreversible metal nanoparticle formation also occurs also with some Cu based covalent frameworks[153] and metal–organic frameworks[154,155] and even with Cu doped carbon structures. For example, one study investigated a copper/nitrogen doped carbon network (Cu$_{0.5}$NC) and found it to be particularly active for C_2H_5OH formation, yielding 55% in 0.1 M CsHCO$_3$ at −1.2 V *vs.* RHE.[156] XANES and EXAFS were again employed to examine the catalytically active species throughout electrochemical reduction. The *operando* XANES analysis showed a change in oxidation state from Cu(II) to Cu(0) whilst the EXAFS data showed the appearance of Cu–Cu bonds, consistent with the formation of copper nanoparticles. The activity of this catalyst is highly comparable to an engineered copper nanoparticle/N-doped graphene catalyst, which also produced ethanol at 63% FE at −1.2 V *vs.* RHE,[157] providing further evidence that the active species in the catalyst is metallic copper.

However some catalysts, such as a self-assembled cuprous coordination polymer (Cu-SCP), are reported to be stable towards the formation of metallic Cu(0) nanostructures.[153] The persistence of the Cu(I) oxidation state throughout catalysis is proposed to be responsible for superior C_2 production, which reached a maximum of 33.5% for C_2H_5OH and 19.7% for C_2H_4. The hydrophobicity of the ligand was increased by adding phenyl groups, which was proposed as a strategy for suppressing the HER whilst increasing the production of the crucial *CO intermediate. XAS measurements pre and post electrolysis show no change in state of the copper, however a lack of *operando* measurements makes it difficult to confirm that metal nanoparticle formation isn't occurring reversibly under catalytic conditions.

Overall, the number of studies of transition metal complexes that act either as catalysts or pre-catalysts for ECO_2R to C_{2+} products is relatively low when compared to the level of research on metallic Cu electrodes. However, there is a large number of
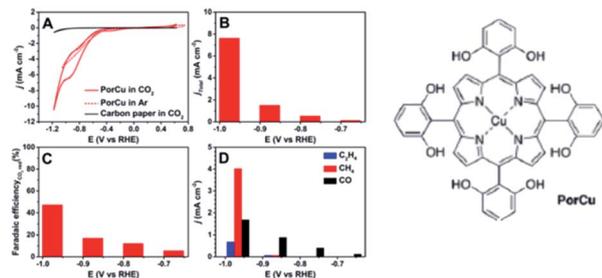
transition metal complexes known to be able to reduce CO_2 to CO and a recently reported new approach to C_{2+} production is to immobilize these on Cu surface.[50] The aim is to produce CO, a crucial intermediate for C_{2+} products, at high turnover frequency and selectivity using the molecular catalyst, prior to CO reduction on Cu. This tandem approach is analogous to that described in Section 2.1.1 that explores the combining of copper with CO producing metals. The only example of a tandem system using a molecular catalyst is reported by Sargent et al.,[50] in which a copper surface is functionalized with 5,10,15,20-tetraphenyl-21H,23H-porphine iron(III) chloride (FeTPP[Cl]), a well-established CO_2 to CO molecular catalyst.[158] A peak FE for C_2H_5OH of 41% was reached at −0.82 V vs. RHE, significantly out-performing bare Cu at 29% FE. The partial current density was 124 mA cm^{-2}. In situ XAS showed the FeTPP to be stable against metallic Fe nanocluster formation under electrochemical conditions.

More widely, surface modifications of Cu electrodes with molecular species have shown success in promoting C_{2+} selectivity. Glycine has demonstrated impressive enhancement of C_2H_4 and C_2H_6 production on copper nanowires (Cu NW) across the entire studied potential range (−0.65 to −1.25 V vs. RHE), doubling their FE at −1.25 V to 35%.[59] A noteworthy limitation of the catalyst is the stability of the adsorbed glycine, which will detach at potentials more negative than the studied range. A range of morphologies was investigated with all showing an enhancement in the presence of the glycine adsorbates. DFT calculations reveal stabilization of the *CHO intermediate, key to the formation of hydrocarbons, by glycine's −NH_3^+. N,N′-Ethylene-phenanthrolinium dibromide has been utilized to synthesize and stabilize nanostructured copper from planar polycrystalline foil, shifting the selectivity to C_{2+} products including C_2H_4 (FE = 45%) and C_2H_5OH (FE = 15%) at moderate potential (−1.05 V vs. RHE).[159] The additive first corrodes the surface of the foil to form the nanostructure and then dimerises under applied potential to form a film which was shown to stabilize the structure for over 40 hours. Altering the C_2 pathway to preferentially form C_2H_5OH over C_2H_4 has been explored using a nitrogen-doped carbon layer coated onto copper.[160] DFT studies give evidence towards to simultaneous improvement in C–C coupling and suppression of deoxygenation of the fork-in-the-road HOCCH* intermediate which is a necessary step for the formation of C_2H_4. C_2H_5OH is selectively produced at 52% FE at, crucially, an industrially relevant partial current density of 156 mA cm^{-2} at −0.68 V vs. RHE.

2.3 Photoelectrodes and photocatalysts

Indirect solar CO_2 reduction, where a photovoltaic is used to enable dark electrocatalysis with metal electrodes, is increasingly reported, but is not discussed here as the achieved product distribution invariably aligns with that achieved with the electrode material used conventionally. Instead, we briefly examine the reduction of CO_2 to C_{2+} products using either semiconductor photocatalysts or photoelectrodes that generate suitably reducing photoelectrons to enable CO_2 reduction at a catalytic site.

Perhaps surprisingly, given the need to accumulate very large numbers of photoelectrons at a catalyric site (e.g. the production of ethane from CO_2 is a 14-electrons process), and the typically low quantum yields of most photocatalysts coupled to the available solar flux, examples of materials that convert CO_2 to C_{2+} products do exist. These are included within a comprehensive recent review on CO_2 photoelectrodes and photocatalysts,[161–166] where it is noted that when metal co-catalysts are deposited on the light absorbing semiconductor the achieved selectivity often matches that expected for the material with Cu co-catalysts often giving rise to a distribution of products including ethane and other C_2 molecules. Highlights of Cu catalyzed systems include reports of p-Si nanowires with Cu deposited on the surface for the production a range of C_2–C_4 products,[167] PbS sensitized TiO_2 particles with Cu co-catalysts[168] that could produce C_2H_6 in the presence of CO_2 and bimetallic alloys of Pt/Cu on TiO_2 for the production of C_2H_6 and C_2H_4.[169]

Cu containing photoelectrodes have also been reported to produce complex carbon products without the need for an additional co-catalyst, likely due to the availability of active Cu sites on the electrode surface.[170–173] Selected examples include one-dimensional Cu_2O@Cu metal–semiconductor heterostructured nanorods that produced C_2H_4.[172] The reduction of CO_2 to acetic on CuO photoelectrodes where the formation of thin surface films of Cu–In that inhibited H_2 evolution and promoted C_2H_5OH production.[174] Also a study where very high selectivity's towards C_2H_5OH was reported using a CuO/Cu_2O photocathode with a micro-flow reactor which appeared to have an essential role in controlling pH and local CO_2 concentration.[175]

Several studies do exist where non-Cu based co-catalysts have been used.[176–179] In two reports[180,181] Pd–TiO_2 was shown to produce ethane under CO_2 and in the presence of water, particularly at low temperature.[180] Plasmonic Au nanoparticles are also proposed to be able to act as both the light absorbing and catalyst centre for C_2H_6 production from CO_2,[182] and although not containing a C–C bond, methyl formate production via the photoelectrochemical reduction of CO_2 at InP electrodes can occur.[183]

Although both electro- and photocatalytic CO_2 reduction offer efficient techniques for C_2 products conversion, the reduction of CO_2 to C_{2+} products, such as C_3 are rarely reported.[184] Moreover, the long-term stability of the widely used transition metal-based catalysts is still under investigation.[185] Biological CO_2 conversion as a cost-effective approach brings new opportunity to generate more complex chemical compounds than purely electrochemical methods. The excellent stability of bio-catalysts and the high coulombic efficiency of CO_2 conversion make it a potentially scalable technology for CO_2 utilization in the circular bioeconomy and high-value biofuel generation (Table 2).[185,186]

2.4 Biological catalysts

2.4.1 Biocatalysts involved in microbial electro-synthesis (MES): pure cultures vs. mixed communities. The conversion of CO_2 in MES systems can be driven by two major types of

Table 2 CO_2 electroreduction by microorganisms in MES compared to electrocatalysts for C_{2+} products

Product	Catalyst	Potential (V vs. Ag/AgCl)	Current density (mA cm^{-2})	Production rate (g m^{-2} h^{-1})	FE (%)	Operation time (h)	Ref.
Acetate	Mixed microbial consortium	−1.3	20	55.4	99	1680	187
	Mo$_8$@Cu	∼−1.85	110	N.G.	48.7	3	188
Ethanol	Clostridium ljungdahlii ERI-2	−0.78	0.19	0.25	66.1	168	189
	B, N-codoped nano diamond	∼−1.65	N.G.	7.2×10^{-5}	93.2	3	40
Mixed alcohols	Mixed microbial consortium	−1.0	∼1.0	0.15	[a]49.5: ethanol, butanol and organic acid	2160	190
	Mesoporous metallic Cu	∼−1.65	18.5	N.G.	35: ethanol and propanol	1	21

[a] Coulombic efficiency.

microbial catalysts: mixed cultures and pure cultures. From a general point of view, chemolithoautotrophic bacteria are of interest for MES because of their ability to fix CO_2 using hydrogen in addition to their electroactivity towards CO_2 reduction.[191,192] When it comes to pure cultures and the production of C_2 to C_6 compounds from CO_2 reduction, acetogens are the most studied microorganisms because of the acetate as a natural product from the Wood–Ljungdahl (W–L) pathway. In addition, the W–L pathway is the most energetically efficient known pathway for CO_2 as more than 95% of carbon and electron flow is diverted to the production of extracellular end-products, rather than to the microbial growth and biomass production.[193] A wide range of acetogens are able to accept electrons from a cathode and use CO_2 as a terminal electron acceptor, such as *Sporomusa*, *Clostridium*, *Acetobacterium*, *Desulfovibrio*, *Sulfurospirillum*, and *Moorella thermoacetica*.[193,194] The exact mechanisms for the electron transfer (*i.e.*, direct or indirect/mediated) are, however, still hypothetical and highly depend on operating conditions. In order to specifically target compounds with a higher value than acetate, genetic engineering of acetogens can also be considered.[195–197] This can, for example, be achieved by eliminating genes responsible for the production of acetate and ethanol and by introducing or over-expressing genes essential for the production of the targeted commodity in *Clostridium* sp. in order to favor a specific pathway.[198]

In order to develop a robust process at a larger scale, mixed microbial communities will be preferred as they are more robust and versatile, but also easier to handle. Besides, mixed microbial communities can be directly enriched from environmental samples such as activated or digested sludge, anaerobic digester effluents or river sediments.[199–203] In a controlled environment such as in Bio-Electrochemical Systems (BES) and the presence of methane inhibitor, the enrichment of acetogenic bacteria from environmental inocula was very often reported, which is consistent with the production of Volatile Fatty Acids (VFAs) and alcohols. For example, it was reported in several studies that organisms belonging to the genus *Clostridium* and *Acetobacter* dominated both the biofilm and the planktonic microbial communities of a BES producing VFAs and alcohols from CO_2 conversion.[198,204,205] The presence of *Desulfovibrio* species was also reported.[206–209] This could be explained by their implication in biological hydrogen production in biocathodes and would thus support the thesis of a hydrogen-mediated mechanism.[209–211] In our latest study, the activated sludge from a wastewater treatment plant was used as inoculum for MES which was poised potential of −1.0 V *vs.* Ag/AgCl and provided only gaseous CO_2. A dense biofilm dominated by *Acetobacterium* (*ca.* 50% of biofilm) was gradually formed to produce a higher yield of acetate (106.9 ± 10.5 mM). The sharp drop of charge transfer resistance within the biofilm highlighted the advantage of mixed communities. In addition, the biofilm maintained a highly active performance during long-term operation even with the stress associated with the low pH as a result of accumulation of acidic products.[204] Changing the operation from batch to continuous mode (hydraulic retention time of 3 days) further promoted the acetate production as it provided better control of pH and constant medium refreshment.[212]

2.4.2 Main challenges and bottlenecks of BES. Over the past 10 years, the scientific community has gained increasing knowledge about microbial electrosynthesis and the production of chemicals from CO_2 reduction.[186,213] All the studies reported have been carried out at a laboratory scale. There is still a long way to go in order to develop a viable technology at a larger scale and there are some challenges to be tackled. Firstly, the exact mechanisms of electron transfer and bacterial interaction with solid-state electrodes are still to be elucidated. In most of the studies reported in the literature, the potentials applied to drive the bioelectrochemical reduction of CO_2 are lower than the theoretical H_2 evolution potential (−0.414 V *vs.* SHE).[214] Moreover, understanding the exact role of the biofilm growing at the electrode is also of major importance, as it is likely that the biofilm catalyses H_2 evolution rather than the reduction of CO_2 directly. The development of a robust and selective biocatalyst to target a specific product with high productivity is another challenge in MES. First of all, in the case of the production of VFAs, there is a competition with methanogens that needs to be

prevented. In addition, the enrichment of a community with desired characteristics for MES, such as facultative, autotrophic, electro-active and biofilm forming[193] is a long process (usually between 50 and 100 days). Efforts should be pursued towards the production of compounds of higher value *via* MES. Most recent studies have highlighted the production of VFAs and alcohols up to C_6. Increasing titers, productivity and purity will be the keys to the development of an attractive and economically viable technology. Finally, to date, no study has been carried out at the pilot scale which shows that MES is still far from being a mature technology.

2.4.3 Integration of MES with other technologies: the case of bioplastics production. With acetate and butyrate as metabolic precursors, compounds even more complex than C_{2+} VFAs and alcohols can be targeted, especially if MES is combined with other technologies. It is, for example, the case of polyhydroxyalkanoates (PHAs), which are bioplastics that have attracted increasing interest because they are biodegradable and mainly produced from renewable sources such as organic acids or wastes.[215–219] Indeed, it was shown that MES can be involved in a three-step process for the production polyhydroxybutyrate (PHB) from CO_2.[220] In this process, MES was used as a first step to accumulate 43.7 and 103 mmol of acetate and butyrate, respectively. In a second step, acetate and butyrate were extracted and concentrated by membrane extraction with a concentration of 400 mM (of which 65% butyrate). Finally, during the last step, PHB was accumulated in an aerated bioreactor operated in fed-batch and using inoculum previously enriched in a sequencing batch reactor (SBR). A maximum of 74.4 g PHB per 100 g volatile suspended solids (VSS) was produced, for an equivalent carbon conversion of 0.41 kg of PHB obtained for 1 kg of carbon as CO_2 inlet to the entire system.[220] Combining MES with other technologies for extraction and elongation like fermentation makes sense as the production of complex compounds such as bioplastics does not seem realistic *via* MES only.[221–223] However, the combination of MES with fermentation should be clearly distinguished from electrofermentation (EF) in which the role of the electrode (and electrons) is very different. Indeed, EF is a spontaneous fermentation process influenced electrochemically whereas MES relies on the reducing power provided to drive a non-spontaneous reaction.[220] It was, for example, reported in a study focusing on butanol production that only 0.2% of the cathodic electrons were used for the production of butanol whereas 99.8% originated from the glucose substrate.[224]

2.4.4 Bio-electrochemical systems for longer chain production. BES is based on the capacity of specific strains of bacteria to electrochemically interact with solid-state electrodes. More specifically, during MES, electrophilic microorganisms can accept electrons from a polarized electrode (directly or indirectly) for their own growth and maintenance but also reduce CO_2.[225–227] It should be understood that MES relies on the external power applied at the cathode to drive the non-spontaneous CO_2 reduction. Unlike in fermentation or EF processes, there is initially no other electron donor than the cathode in MES. During the last few years, research studies have

demonstrated the potential of MES for the conversion of CO_2 into C_2 to C_6 VFAs and alcohols.[228–232]

2.4.5 Production of C_2–C_6 compounds *via* microbial electrosynthesis. Besides the production of methane (CH_4), which is considered as a competitive reaction when it comes to the production of VFAs or alcohols *via* MES, acetate ($C_2H_3O_2^-$) is the main C_2-product from CO_2 conversion in BES. Indeed, when BES reactors are inoculated with environmental samples such as activated sludge or sediments, the bacterial community growing in the medium and in the biofilm, if there is one, will quickly be dominated by methanogens and acetogens.[198] As the production of methane must be avoided in order to favor VFAs and alcohols, inhibition methods are often used at least at the beginning of the process. They include chemical inhibitors such as sodium 2-bromoethanesulfonate, inoculum heat pretreatment or pH control. In the W–L pathway, acetogens reduce CO_2 to conserve energy and for the synthesis of cell carbon, but also to synthetize acetyl-CoA and then acetate.[233] Acetate is the natural product from acetogenesis and has therefore been the focal point of numerous studies.[234] Under standard conditions, CO_2 may be reduced bioelectrochemically to acetate at a potential (E^0) of -280 mV *vs.* SHE (eqn (1)), but no electroacetogenesis was reported with a biocathode poised at such potential.

$$CO_2 + 7H^+ + 8e^- \rightarrow$$
$$CH_3COO^- + 2H_2O; E^0 = -280 \text{ mV } vs. \text{ SHE} \quad (1)$$
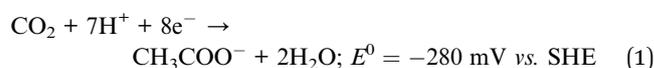
It is well understood that potential losses occur in BES. These losses are related to mass transport and kinetics limitations between the medium, the electrode and within the biofilm (when applicable), but also to ohmic voltage losses associated with the electrolytes, the membrane, the electrodes and connections. Therefore, it has been postulated that in order to overcome potential losses due to the components of BES, microbial acetogenesis requires potentials of -400 mV or much more negative.[204,235–237]

In order for the technology to be viable, reaching high productivity and selectivity is crucial. Therefore, different strategies have been investigated to increase the acetate production rate, ultimately limited by the applied current. For example, the continuous production and extraction of acetate were achieved in a 3-compartment microbial electrolysis cell (applied current of -50 mA) reaching an accumulated acetate concentration of 13.5 g L^{-1} (225 mM).[208] In this design, the middle chamber was used for the continuous extraction of acetate which led to the high titer achieved. Electrode materials have also been subject to investigation with the utilization of reticulated vitreous carbon (RVC) modified with multi-walled carbon nanotubes (MWCN) by electrophoretic deposition (EPD).[238] In this reactor polarized at -0.85 V *vs.* SHE, a high acetate production rate of 685 ± 30 g m^{-2} day^{-1} was achieved (product titer of 11 g L^{-1}), which is according to the authors comparable to productivity levels of industrial fermentation processes.[239] However, this experiment was carried out at a very small scale (electrode projected surface area of 1.36 cm^2), and extrapolating such results is not straightforward despite the

high productivity obtained. In addition, the viability of such electrode materials at a larger/industrial scale should be evaluated by economic and life cycle assessment analysis.

Although, as an end-product, it does not have a high market value (ca. 500€ per t),[239] acetate and more specifically acetyl-CoA are excellent building blocks for the production of more valuable chemicals through the W–L pathway.[193,240–242] Therefore, under specific conditions of pH and hydraulic retention time and following mechanisms derived from the W–L pathway, butyrate, ethanol, or butanol can be all produced from acetyl-CoA as a precursor (see Fig. 4a). Ethanol is an important biofuel and can be used as an additive to diesel. Butanol is an important industrial bulk as well as a promising biofuel as it can be used without modifications of car engines.[236,243,244] In the W–L pathway, acetate is the prerequisite for any other VFA or alcohol, following which butyrate can be produced either via a linear extension of the acetyl-CoA to butyril-CoA, or via reverse β-oxidation which is also called microbial chain elongation (Fig. 4b).[234]

As acetate and butyrate concentrations increase in the medium, pH will naturally drop creating harmful conditions for microorganisms. As a defensive mechanism, a switch of mechanism from acidogenesis (production of fatty acids) to solventogenesis (production of solvents, typically alcohols) can occur, leading to the production of butanol and ethanol.[246] Concomitant of the production of butanol and ethanol, acetone can also be produced via acetone–butanol–ethanol (ABE) fermentation, which can be further reduced to iso-propanol via isopropanol–butanol–ethanol (IBE) fermentation.[246] This mechanism, however, has rarely been reported in bioelectrochemical systems. During MES, operating parameters such as applied potential, pH or hydraulic retention time (HRT) have a crucial impact on the bioproduction. In a continuous reactor operated at −50 mA (cathode potential of −1.0 ± 0.6 V vs. SHE), it was shown that the bioproduction could be driven either towards acetate or towards product diversification by controlling the HRT and thus the pH.[209] At HRT of 3.3 days, a production rate of 21 g $m_{cathode}^{-2}$ d^{-1} could be achieved for acetate with very low product diversification. Higher HRT of 5 days enhanced the production of butyrate and isopropanol as
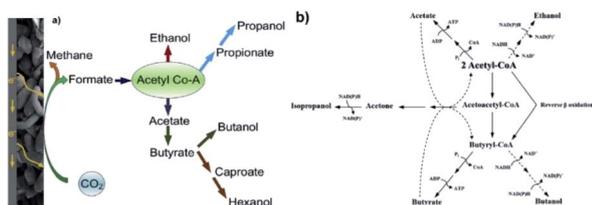
the pH would drop to 5, with maximum concentrations of 0.67 and 0.82 g L^{-1}, respectively. In another semi-batch reactor operated for 450 days at an applied cathode potential of −0.80 V vs. SHE and with controlled pH ca. 5, the accumulation of acetate up to 4.9 g L^{-1} also led to the production of ethanol (up to 1.3 g L^{-1}).[209] As observed in other studies, the presence of both acetate and ethanol led to both solventogenesis and chain elongation. Therefore, high butyrate and isobutyrate titers of 3.1 and 1.6 g L^{-1} were measured. Caproic acid was also detected, reaching a maximum concentration of 1.2 g L^{-1} after 450 days of operation. Equivalent alcohols were produced: in addition to ethanol, butanol, isobutanol and hexanol were measured as high as 0.4, 0.2 and 0.2 g L^{-1}, respectively.[206] More recently, the system was adapted to a 3-chamber MES rector equipped with a dual biocathode arrangement for sequential acetogenesis/carbon chain elongation and solventogenesis, as presented in Fig. 5.[206] In this study, the pH of both biocathode chambers were controlled without the addition of any chemicals but CO_2 sparging and by controlling the applied potential and the abiotic reactions occurring at each cathode. In the first chamber (pH 6.9), acetate could be produced at a maximum concentration of 9.5 g L^{-1} (0.46 g L^{-1} day^{-1}). As acetate would migrate to the second chamber (pH 4.9), solventogenesis would occur and ethanol would be produced. Very interestingly, after a connection was made between the headspaces of both cathodic chambers, a transfer of ethanol from the second chamber to the first chamber via gas stripping promoted chain elongation in the first chamber. C_{4+} products were then detected with levels up to 1.33 g L^{-1} isobutyrate, 1.49 g L^{-1} butyrate and 0.27 g L^{-1} caproate. Acidic conditions in the second chamber resulted in the biosynthesis of C_4–C_6 alcohols, with levels up to 0.33 g L^{-1} isobutanol, 0.82 g L^{-1} butanol and 0.11 g L^{-1} hexanol.[247]

It is assumed that additional electron donors than a polarized cathode was required to steer the production towards longer chain of carboxylates than acetate.[248] Based on our latest

Fig. 4 (a) Possible metabolic pathways for microbial electrochemical CO_2 reduction that leads to the generation of a variety of high value organic compounds beyond acetic acid and CH_4.[224] Reproduced from ref. 224 with permission from Elsevier, copyright 2019. (b) Schematic diagram of the suggested metabolic pathways for the production of acetate, ethanol, acetone, isopropanol, butyrate and butanol from acetyl-CoA. In dashed lines are the pathways for solventogenesis after the production of acetate and butyrate.[245] Reproduced from ref. 245 with permission from Elsevier, copyright 2012.

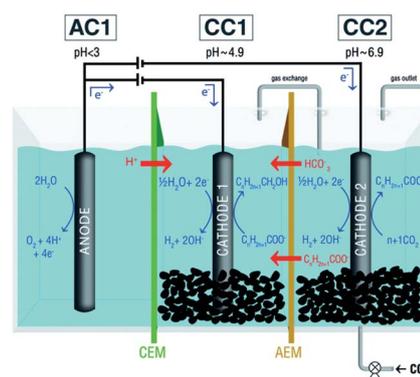Fig. 5 Schematic representation of a microbial electrosynthesis reactor with dual biocathode for the production of organic acids at neutral pH and simultaneous reduction of the produced organic acids to the corresponding alcohols at mildly acidic pH. CEM: cation-exchange membrane; AEM: anion exchange membrane.[247] Reproduced from ref. 247 with permission from the Royal Society of Chemistry, copyright 2019.

results, formate as additional electron donors were supplied into MES in which cathode was poised at −1.0 V *vs.* Ag/AgCl. Although acetate was still the major product, significant increase in the production of butyrate (3.8 times higher in maximum concentration) and butanol (maximum of 6.8 ± 0.3 mmol C L^{-1}) was observed after supplying formate. However, the production of acetate and longer chain carboxylic acids ethanol stopped at open circuit condition. By comparison, ethanol as another one electron donor could trigger the C$_4$ compounds production without polarized cathode.[237]

3. Reactor design

3.1 Reactor configurations and process integration

The design of a CO$_2$ electrochemical reduction device requires multi-disciplinary efforts. Among the three sources of inefficiencies in ECO$_2$R, which are kinetics, mass and charge transfer, potential losses caused by mass and charge transfer are closely determined by reactor configuration. The priority of device design is minimizing those energy losses as much as possible. To date, the most studied devices for ECO$_2$R are membrane-based architectures. These are used in order to avoid cross over of products and the undesired consequent parasitic effects, *e.g.* ion-exchange membranes are employed to separate the catholyte and anolyte while maintaining the transfer of ion transfer across the membrane at the same time. According to the pH environment of electrolyte, cation-exchange or anion-exchange membranes can be used.

In the studies of ECO$_2$R at lab-scale, batch type reactors, shown in Fig. 6, are widely used in favor of precise control of reaction conditions and product characterization. In order to upscale the process, continuous flow configurations are designed to meet the demands of industrial applications as shown in Fig. 6. It is suggested by Delacourt *et al.* that a buffer

layer is crucial to stabilize the pH of catholyte, and thus enhance the selective reduction of CO$_2$ and prevent the evolution of hydrogen.[249] However, due to the limited solubility of CO$_2$ (1.5 g L^{-1} (ref. 250)) in aqueous solutions, flow cells fed with saturated CO$_2$ electrolyte suffer from depletion of reagent showing a low mass transfer limiting current density at around 20 mA cm^{-2}.[251] Inspired by fuel cell configuration, the gas diffusion electrode (GDE) is integrated into the electrolyzer to enable direct gas CO$_2$ feeding to overcome the mass transfer limitation of the reactant.[252] By doing so, the operating current density reaches 10^2 to 10^3 mA cm^{-2}.[253–255] One can find a more detailed development of GDE for ECO$_2$R as reported in a recent review.[256] Besides, the rapid removal of reductive products along with CO$_2$ stream lowers the issues arising due to ohmic loss caused by the bubble formation in the channel.

However, the use of mono cation or anion exchange membrane requires the consistency of the pH environment across the membrane. This brings a performance trade-off on anode and cathode because of the conflicting electrolyte requirements for desirable half-reactions.[257,258] For example, the alkaline electrolyte is preferred for anodic oxygen evolution reaction (OER) to eliminate the use of catalysts based on precious metal, while there are still plenty of ECO$_2$R attempted at a near-neutral catholyte. The bipolar membrane configuration enables a differential pH environment for each half-reaction, as shown in Fig. 6.[259] The development of bipolar membranes with controlled local pH has been recently reported as one way to use the devices with the CEM in contact with the cathode for CO$_2$ reduction[260] although this configuration requires large membrane potential loss sometimes to drive ion transfer at the membrane, which can lead to the decline of energy efficiency.[261] In addition, the loss of CO$_2$ due to the reaction with OH$^-$ to form CO$_3$$^{2-}$ at the cathode usually needed a large excess of CO$_2$ to support high current densities, which
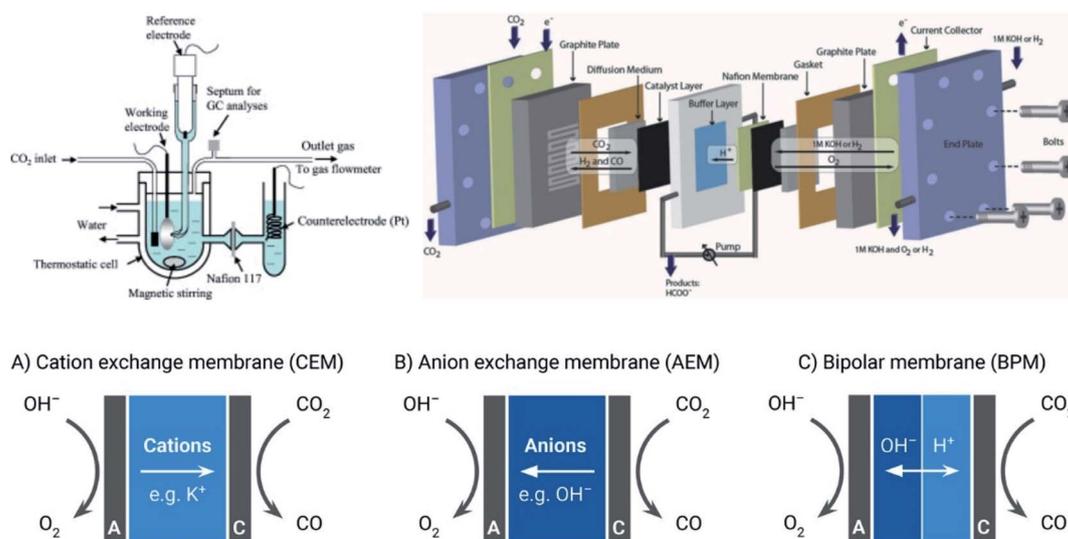

Fig. 6 (Up) The schematic of batch and continuous flow reactor for CRR.[273,274] Reproduced from ref. 273 and 274 with permission from IOP Publishing, copyright 2010 and 2013; (down) ion transport pathways in CEM (A), AEM (B), and BPM (C).[261] Reproduced from ref. 261 with permission from American Chemical Society, copyright 2018.

led to a lower carbon efficiency. BPM provided the possibility for CO_3^{2-} protonation at the membrane–electrolyte interface to release CO_2, reducing the losses imposed by CO_3^{2-} formation.[262] As an alternative to a physical membrane a microfluidic approach was implemented to introduce a thin laminar flow electrolyte layer served as a 'virtual membrane' to separate anode and cathode.[263] High efficiency and precise control of operating conditions make microfluidics a powerful tool to boost the performance of ECO_2R.[264] By employing two GDEs, one as an anode and one a cathode, this configuration is able to utilize gaseous CO_2 and transport byproduct O_2 away. Performing ECO_2R in a solid oxide electrolyzer cell (SOEC) under high temperature is more kinetically desired and energy efficient than room temperature membrane-based ECO_2R configuration.[265] Approximately a 73% energy efficiency and 95% FE was reported by Kaur et al.[266] In addition, SOEC is capable of operating at high current density (up to 2 A cm^{-2}), which is crucial for industrial scale application.[267] More information about SOEC can be found in a recent review.[268]

One of the key concepts of carbon-neutral fuel generation by ECO_2R is that electrical energy comes from renewable sources, like solar and wind energy.[269] Kauffman et al. presented a lab-scale prototype of a solar cell powered CO_2 electrochemical device.[270] The configuration was provided a bias of 6 V by a solar panel and is able to generate 412 L h^{-1} CO with 96% selectivity for 12 h in two days. A much higher production rate of 781 L h^{-1} was detected by using a rechargeable 6 V battery which provides more stable and higher power density electricity. They also estimated the conversion capacity of CO_2 is 1 tonne per acre per day and 1.6 tonnes per turbine per day for solar and wind plants, respectively. ECO_2R based on a SOEC is also regarded as an efficient approach of energy storage for intermittent renewable energy with energy storage cost around 3 kW^{-1} h^{-1}.[271] The integrated system of ECO_2R and following treatment sections like Fischer–Tropsch (F–T) was investigated to provide a technical and economic feasibility study of converting CO_2 back into diesel fuel.[272] It is suggested that this pathway to synthesize fuel can be economically competitive with fossil fuel.

3.2 Operating condition of ECO_2R

Pressurizing CO_2 has been proven an efficient way to promote the electrochemical performance and selectivity of hydrocarbons.[251,275,276] It is considered as a method to improve the solubility and mass transfer of CO_2 at the surface of the electrode.[277] Besides, the reaction rate of ECO_2R can also be accelerated through increasing the concentration of reagent. A desirable high carbon product selectivity is also obtained at pressurized conditions,[278] which means the local concentration of CO_2 plays a critical role in C_{2+} generation, as shown in Fig. 7. The study of Kas et al. indicated that the FE of C_2 rises by about three times to 43.7% at a pressure of 9 atm.[279] It is also suggested that high pressure can result in the polymerization of low carbon products.[280]

The temperature effect on ECO_2R depends on the type of electrolyte. In organic electrolytes, like CH_3OH, a low temperature to maintain a higher solubility of CO_2.[281] In contrast, rising

in temperature leads to performance improvement in aqueous electrolyte due to the improvement on kinetics, despite modest reductions in the solubility of CO_2.[38] Dufek et al. reported a rise and fall effect of temperature in current performance and product selectivity.[282] The results from the study of Gutiérrez-Guerra et al. suggested that higher operating temperature is preferred for high carbon products generation.[283]

3.3 Electrolyte

As already shown in this review, the selection of electrolytes is a crucial factor for ECO_2R. Product distribution is heavily affected by the properties of electrolyte e.g. pH, protic vs. aprotic and CO_2 solubility. In addition, to conventional electrolytes, ionic liquids (ILs) have garnered much attention for ECO_2R in recent years.

ILs are a novel class of liquids, made up solely of ions which possess a unique set of properties. These properties, such as chemical tunability, high stability, low vapour pressure, large liquidus temperature range and wide electrochemical window make them useful in a number of applications.[284] ILs have also been shown to exhibit superior gas sorption/capture capacity in comparison to organic solvents.[285] The tunability of ILs has allowed the design of ILs to capture greater than equal molar amounts of gas.[286] For ECO_2R the large CO_2 capture potential of ILs is advantageous and, additionally, the ability to chemically absorb CO_2 can in some cases lead to activation of CO_2 for ECO_2R.[287]

Many reports of ILs used for electrocatalytic reduction of CO_2 exist but products reported are mainly C_1 type compounds.[288] Only a small number of papers report the production of C_{2+} compounds and in most cases the IL is acting as a co-catalyst rather than an electrolyte. In all of the cases reported the IL has been paired with a copper type catalyst to produce C_{2+} products. Sun et al. showed the conversion of CO_2 to acetic acid at 80.3% FE when Cu(I) and a carbon-doped boron nitride catalyst was used alongside a LiI-water-IL electrolyte where the IL used was 1-ethyl-3-methylimidazolium tetrafluoroborate ([Emim][BF$_4$]).[289] Hui et al. showed the incorporation of IL (1-octyl-3-methylimidazolium chloride, OmimCl) into a Cu_2O supported on a graphite sheet catalyst could more than double the FE of C_2H_4.[290] Another group reports the production of C_2H_5OH at a rate of 24.42 μmol cm^{-2} h^{-1} at a potential of −1.6 V vs. Ag/AgCl (KCl sat.) using a combination of copper nanofoam and an electrolyte of 0.1 M $KHCO_3$ + 0.04 M 1-butyl-3-methyl-imidazolium bromide (BmimBr).[291]

The limited reports in the literature would suggest that the utilisation of ILs to produce C_{2+} products has been largely unexplored. However, these reports also outline the potential of ILs to enhance production and selectivity to C_{2+} products. Most reports on C_{2+} conversion to date focus on imidazolium based ILs, therefore, there is a large variety of ILs which remain unstudied. It is estimated that there are potentially a million different ILs available[284] with diverse properties including those which reactively solubilise CO_2. Therefore, it is highly likely that ILs could hold the key to going beyond C_1 products and should be studied more closely for this application.
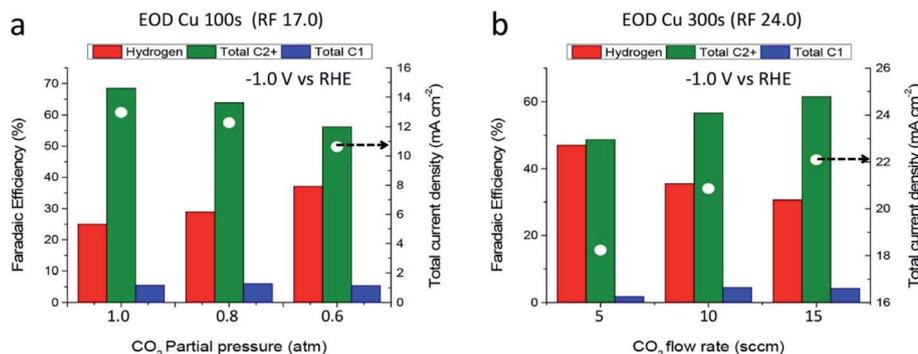
Fig. 7 Products distribution and current performance with CO_2 pressure (a) and flow rate (b).[278] Reproduced from ref. 278 with permission from American Chemical Society, copyright 2017.

4. Perspectives

4.1 Catalyst design and development

Understanding the catalytic mechanism and catalyst design if one wants to improve the yields of C_{2+} products, then there should be efficient C–C coupling steps. Perhaps the most efficient manner to advance in the intelligent design of catalysts is to understand the reaction mechanism and identify and analyze the limiting factors.

4.1.1 Catalyst design to promote CO generation. Goddard and co-workers found that on Cu(111) the CO dimer pathway is less favourable than the formation of an adsorbed COH* followed by C–C bond formation by reaction of this species with adsorbed CO*.[292] However, in a separate study using explicit water on Cu(100), this group found that the reaction to form adsorbed CHO*, as opposed to COH, was preferred. Other computational studies on Cu has shown that adsorbed CH_xO^* ($x = 0–3$) dissociation to CH_x as well as CH_xO^* insertion to CH_x needs to surmount a much larger barrier on pure Cu.[293] These findings suggest that CO_2 reduction is not likely to give rise to C_{2+} through the CO* intermediate. Nevertheless, based on the fact that adsorbed species HCOO*, H_2COO^*, HCOOH, and H_2COOH are difficult to couple with each other or other intermediates, the most promising approach to achieve large-scale long-chain carbon fuel production is modified Fischer–Tropsch (F–T) synthesis, perhaps with synergetic effects on Co- and Ru-based catalysts. Therefore, to promote the synthesis of C_{2+} products (hydrocarbons and alcohols), future efforts should focus on discovering new catalysts that promotes CO generation from CO_2/H_2, C–O bond dissociation from CH_xO^* and CO*/CHO* insertion to CH_x simultaneously.

4.1.2 Catalyst design through DFT and computational tools. Computational modelling opens a rational way to design catalysts, examples of catalyst design by means of density functional theory (DFT) have already emerged.[294,295] Using DFT theoretical works, the scaling relations between characters of catalysts and the reaction to intermediates are discovered. In Nørskov's study, over 20 types of catalysts including metals, metal oxides, cation-exchanged zeolites, decorated graphene nanosheets and metal–organic frameworks have been selected to construct the scaling relationships for C–H bond activation

reactions.[296] DFT combines the structure of active sites with catalytic performance, making it possible to design catalysts by constructing specific active sites. It was found that the Cu clusters exposed more coordination unsaturated surface atoms in the form of angular and edge atoms which strengthened the adsorption of the reaction intermediates calculated by DFT.[297] Another example is to construct metal-N sites, it is proposed that the special electronic structure of the coordinated metals in single-atom catalysts would be able to efficiently promote C–C coupling.[184,298] DFT could also be used to predict the performance of metal-free catalysts. Both experiments and DFT calculations demonstrated that the special pore structures and pyridinic/pyrrolic N sites were crucial for CO* dimerization and C_2 compounds conversion.[299]

Despite computational tools being extremely useful to describe reaction mechanisms, they are still far from accurately considering all the processes included in an electrochemical reaction. There are several intrinsic shortcomings of DFT methods (commonly used) in describing the energies of several reaction intermediates, for example, (i) overestimation or underestimation of CO and CO_2 adsorption energies on transition metal-based catalysts when using DFT instead of DFT+U, especially in semiconductors;[300] (ii) overestimation of CO_2 hydrogenation energy.[301–303] Improved methods to describe electrochemical reactions in-depth need to consider the following aspects within a dynamic characteristics of the Helmholtz double-layer: (i) an electrochemical phase diagram as a function of the applied potential;[304] (ii) the modified Poisson–Boltzmann approach for Tafel lines generation;[305] (iii) constant-charge or constant-potential, which is better in modeling the electrolyte–catalyst interface (electrochemical double layer); and (iv) cyclic voltammetry curves simulation using KMC and microkinetic methods.[17]

4.1.3 Synergetic effects to promote C–C bound from hybrid catalysts. The limited literature relating to molecular electrocatalysts for the reduction of CO_2 to C_2 or higher products highlights the challenging nature of the goal and major barriers to success that exist. Specifically, the majority of molecular catalysts are initially developed in solution, prior to heterogenization, and they contain a single binding site. Therefore

facilitating C–C bond formation through the coupling of two M–CO sites, in a manner analogous to that proposed to occur with metal electrodes,[306] is challenging. In solution, the chance to encounter two suitably orientated and long-lived partially reduced intermediates is unlikely. Kinetic limitations may lead to the formation of C_1 products even if the thermodynamically favored pathway is for C–C bond formation. Furthermore, the transient nature of the interaction of the catalyst with the electrode itself, coupled with the common usage of only one or two redox-active sites per catalyst makes the generation of highly reduced products difficult. The three classes of catalysts described above overcome these fundamental limitations using differing, but equally valid approaches. Firstly, the catalysts for oxalate formation avoid the need to generate highly reduced intermediates at a single catalytic site, instead product formation occurs through bringing together 1-electron reduced CO_2 centres each bound to a separate metal centre. Secondly, studies from Tanaka and colleagues have demonstrated that stabilisation of M–CO intermediates, either through intramolecular interactions or the use of low temperatures, allows for C–C bond formation when a Ru catalyst with a suitable vacant binding site is used. Finally, heterogenized catalysts have been shown to be able to deliver even up to C_3 products. However, it is important to recognize that in many cases the reversible formation of metallic Cu nanoparticles can occur *in situ* and these are likely to be the catalysts.[151] Nonetheless, the dependence of catalytic activity on ligand structure does indicate a pathway by which reactivity can be further tuned. The design of catalysts that can modify the 2nd coordination sphere during catalysis has yielded the most active CO evolving molecular catalysts and the emerging literature on small molecule and polymer surface treatments for Cu electrodes demonstrates that tailoring the local environment at the catalytic centre is a promising avenue of research.

4.2 Eliminating energy loss through process intensification and device innovation

Many efforts have been done on designing and optimizing ECO_2R devices. For room temperature membrane-based devices, the mass transfer limitation of CO_2 is basically resolved through adjusting GDE design.[308] However, the mono ion-exchange membrane (CEM or AEM) restrains the application of different pH environment on cathode and anode. As discussed in Section 3.1, bipolar membrane offer a bright prospect on the manipulation of electrolyte of half-reactions, which enables low cost and flexible choice of electrocatalysts *via* pH differential operations, as suggested by recent numerical studies.[307] Advanced bipolar membranes should be developed to reduce the ion transfer resistance with acceptable performance degradation. For high-temperature SOEC, more research attention should be paid on promoting the product selectivity. We believe pressurized CO_2 and optimized temperature operation guides the future direction of CRR device design, not only because of better mass transfer performance, but also due to the potential to produce high carbon products. Additionally, alternative electrolytes, such as ILs have the ability in catalyzing

ECO_2R. With beneficial properties such as high CO_2 solubility and intrinsic electrical conductivity, ILs are prime candidates to enhance the activity for C_{2+} products, and due to the lack of scientific reports in this area, it is clear there is much work that can still be done.

Abbreviations

CCU	Carbon capture and utilization
ECO_2R	Electrochemical CO_2 reduction
OD	Oxide derived
MES	Microbial electro-synthesis
BES	Bio-electrochemical system
VFA	Volatile fatty acids
EF	Electro-fermentation
W–L	Wood–Ljungdahl
SBR	Sequencing batch reactor
VSS	Volatile suspended solids
RVC	Reticulated vitreous carbon
MWCN	Multi-walled carbon nanotubes
EPD	Electrophoretic deposition
ABE	Acetone–butanol–ethanol
IBE	Isopropanol–butanol–ethanol
HRT	Hydraulic retention time
CEM	Cation-exchange membrane
AEM	Anion exchange membrane
BPM	Bipolar membrane
OER	Oxygen reduction reaction
GDE	Gas diffusion electrode
SOEC	Solid oxide electrolyzer cell
F–T	Fischer–Tropsch
IL	Ionic liquid
PHAs	Polyhydroxyalkanoates
PHB	Polyhydroxybutyrate

Conflicts of interest

There are no conflicts to declare.

Acknowledgements

Notes and references

1 E. R. Delaria, J. Kim, H. L. Fitzmaurice, C. Newman, P. J. Wooldridge, K. Worthington and R. C. Cohen, *Atmos. Meas. Tech.*, 2021, **14**, 5487–5500.

2 M. Grasemann and G. Laurenczy, *Energy Environ. Sci.*, 2012, **5**, 8171–8181.

3 F. Sanchez, D. Motta, A. Roldan, C. Hammond, A. Villa and N. Dimitratos, *Top. Catal.*, 2018, **61**, 254–266.

4 F. Sanchez, M. H. Alotaibi, D. Motta, C. E. Chan-Thaw, A. Rakotomahevitra, T. Tabanelli, A. Roldan, C. Hammond, Q. He, T. Davies, A. Villa and N. Dimitratos, *Sustainable Energy Fuels*, 2018, **2**, 2705–2716.

5 Q. Fan, M. Zhang, M. Jia, S. Liu, J. Qiu and Z. Sun, *Mater. Today Energy*, 2018, **10**, 280–301.

6 R. M. Arán-Ais, D. Gao and B. Roldan Cuenya, *Acc. Chem. Res.*, 2018, **51**, 2906–2917.

7 A. Verdaguer-Casadevall, C. W. Li, T. P. Johansson, S. B. Scott, J. T. McKeown, M. Kumar, I. E. L. Stephens, M. W. Kanan and I. Chorkendorff, *J. Am. Chem. Soc.*, 2015, **137**, 9808–9811.

8 Z. W. Seh, J. Kibsgaard, C. F. Dickens, I. Chorkendorff, J. K. Nørskov and T. F. Jaramillo, *Science*, 2017, **355**.

9 Y. Hori, *Modern Aspects of Electrochemistry*, ed. C. Vayenas, Springer, New York, 2008.

10 C. W. Li, J. Ciston and M. W. Kanan, *Nature*, 2014, **508**, 504.

11 Z. P. Jovanov, H. A. Hansen, A. S. Varela, P. Malacrida, A. A. Peterson, J. K. Nørskov, I. E. L. Stephens and I. Chorkendorff, *J. Catal.*, 2016, **343**, 215–231.

12 E. Bertheussen, Y. Abghoui, Z. P. Jovanov, A.-S. Varela, I. E. L. Stephens and I. Chorkendorff, *Catal. Today*, 2017, **288**, 54–62.

13 Y. Hori, A. Murata and Y. Yoshinami, *J. Chem. Soc., Faraday Trans.*, 1991, **87**, 125–128.

14 J. Yoshihara, S. C. Parker, A. Schafer and C. T. Campbell, *Catal. Lett.*, 1995, **31**, 313–324.

15 J. Yoshihara and C. T. Campbell, *J. Catal.*, 1996, **161**, 776–782.

16 J. A. Rodriguez, J. Evans, L. Feria, A. B. Vidal, P. Liu, K. Nakamura and F. Illas, *J. Catal.*, 2013, **307**, 162–169.

17 A. Roldan, *Curr. Opin. Electrochem.*, 2018, **10**, 1–6.

18 J. K. Nørskov, J. Rossmeisl, A. Logadottir, L. Lindqvist, J. R. Kitchin, T. Bligaard and H. Jónsson, *J. Phys. Chem. B*, 2004, **108**, 17886–17892.

19 M. J. Janik, C. D. Taylor and M. Neurock, *J. Electrochem. Soc.*, 2009, **156**, B126–B135.

20 K. J. P. Schouten, Y. Kwon, C. J. M. van der Ham, Z. Qin and M. T. M. Koper, *Chem. Sci.*, 2011, **2**, 1902–1909.

21 M. Ebaid, K. Jiang, Z. Zhang, W. S. Drisdell, A. T. Bell and J. K. Cooper, *Chem. Inf.*, 2020, **32**, 3304–3311.

22 P.-P. Yang, X.-L. Zhang, F.-Y. Gao, Y.-R. Zheng, Z.-Z. Niu, X. Yu, R. Liu, Z.-Z. Wu, S. Qin, L.-P. Chi, Y. Duan, T. Ma, X.-S. Zheng, J.-F. Zhu, H.-J. Wang, M.-R. Gao and S.-H. Yu, *J. Am. Chem. Soc.*, 2020, **142**, 6400–6408.

23 C. Chen, Y. Li, S. Yu, S. Louisia, J. Jin, M. Li, M. B. Ross and P. Yang, *Joule*, 2020, **4**, 1688–1699.

24 T. H. Phan, K. Banjac, F. P. Cometto, F. Dattila, R. García-Muelas, S. J. Raaijman, C. Ye, M. T. M. Koper, N. López and M. Lingenfelder, *Nano Lett.*, 2021, **21**, 2059–2065.

25 Q. Fan, X. Zhang, X. Ge, L. Bai, D. He, Y. Qu, C. Kong, J. Bi, D. Ding, Y. Cao, X. Duan, J. Wang, J. Yang and Y. Wu, *Adv. Energy Mater.*, 2021, 2101424.

26 J. Santatiwongchai, K. Faungnawakij and P. Hirunsit, *ACS Catal.*, 2021, **11**, 9688–9701.

27 P. Iyengar, M. J. Kolb, J. R. Pankhurst, F. Calle-Vallejo and R. Buonsanti, *ACS Catal.*, 2021, **11**, 4456–4463.

28 P. Shao, W. Zhou, Q.-L. Hong, L. Yi, L. Zheng, W. Wang, H.-X. Zhang, H. Zhang and J. Zhang, *Angew. Chem., Int. Ed.*, 2021, **60**, 16687–16692.

29 L. Ou, Z. He, H. Yang and Y. Chen, *ACS Omega*, 2021, **6**, 17839–17847.

30 H. Li, T. Liu, P. Wei, L. Lin, D. Gao, G. Wang and X. Bao, *Angew. Chem., Int. Ed.*, 2021, **60**, 14329–14333.

31 J. Zhang, Z. Li, S. Xia, T. Zhang, Y. Wang, Y. Wu and J. Wu, *Chem. Commun.*, 2021, **57**, 8276–8279.

32 J. J. Kim, D. P. Summers and K. W. Frese, *J. Electroanal. Chem. Interfacial Electrochem.*, 1988, **245**, 223–244.

33 Y. Hori, A. Murata, K. Kikuchi and S. Suzuki, *J. Chem. Soc., Chem. Commun.*, 1987, 728–729.

34 Y. C. Tan, K. B. Lee, H. Song and J. Oh, *Joule*, 2020, **4**, 1104–1120.

35 P. Zhu, C. Xia, C.-Y. Liu, K. Jiang, G. Gao, X. Zhang, Y. Xia, Y. Lei, H. N. Alshareef, T. P. Senftle and H. Wang, *Proc. Natl. Acad. Sci.*, 2021, **118**, e2010868118.

36 Y. Li, S. H. Chan and Q. Sun, *Nanoscale*, 2015, **7**, 8663–8683.

37 J. D. Goodpaster, A. T. Bell and M. Head-Gordon, *J. Phys. Chem. Lett.*, 2016, **7**, 1471–1477.

38 K. P. Kuhl, E. R. Cave, D. N. Abram and T. F. Jaramillo, *Energy Environ. Sci.*, 2012, **5**, 7050–7059.

39 X. Chen, J. Chen, N. M. Alghoraibi, D. A. Henckel, R. Zhang, U. O. Nwabara, K. E. Madsen, P. J. A. Kenis, S. C. Zimmerman and A. A. Gewirth, *Nat. Catal.*, 2021, **4**, 20–27.

40 Y. Liu, Y. Zhang, K. Cheng, X. Quan, X. Fan, Y. Su, S. Chen, H. Zhao, Y. Zhang, H. Yu and M. R. Hoffmann, *Angew. Chem., Int. Ed.*, 2017, **56**, 15607–15611.

41 J. Li, A. Xu, F. Li, Z. Wang, C. Zou, C. M. Gabardo, Y. Wang, A. Ozden, Y. Xu, D.-H. Nam, Y. Lum, J. Wicks, B. Chen, Z. Wang, J. Chen, Y. Wen, T. Zhuang, M. Luo, X. Du, T.-K. Sham, B. Zhang, E. H. Sargent and D. Sinton, *Nat. Commun.*, 2020, **11**, 3685.

42 M. Jouny, G. S. Hutchings and F. Jiao, *Nat. Catal.*, 2019, **2**, 1062–1070.

43 Y. Hori, I. Takahashi, O. Koga and N. Hoshi, *J. Phys. Chem. B*, 2002, **106**, 15–17.

44 Y. Zhou and B. S. Yeo, *J. Mater. Chem. A*, 2020, **8**, 23162–23186.

45 H. Bai, T. Cheng, S. Li, Z. Zhou, H. Yang, J. Li, M. Xie, J. Ye, Y. Ji, Y. Li, Z. Zhou, S. Sun, B. Zhang and H. Peng, *Sci. Bull.*, 2021, **66**, 62–68.

46 H. Li, Y. Li, M. T. Koper and F. Calle-Vallejo, *J. Am. Chem. Soc.*, 2014, **136**, 15694–15701.

47 Y. Hori, I. Takahashi, O. Koga and N. Hoshi, *J. Mol. Catal. A: Chem.*, 2003, **199**, 39–47.

48 Y. Wang, J. Liu and G. Zheng, *Adv. Mater.*, 2021, 2005798.

49 Y. Wang, Z. Wang, C.-T. Dinh, J. Li, A. Ozden, M. Golam Kibria, A. Seifitokaldani, C.-S. Tan, C. M. Gabardo, M. Luo, H. Zhou, F. Li, Y. Lum, C. McCallum, Y. Xu, M. Liu, A. Proppe, A. Johnston, P. Todorovic, T.-T. Zhuang, D. Sinton, S. O. Kelley and E. H. Sargent, *Nat. Catal.*, 2020, **3**, 98–106.

50 F. Li, Y. C. Li, Z. Wang, J. Li, D.-H. Nam, Y. Lum, M. Luo, X. Wang, A. Ozden, S.-F. Hung, B. Chen, Y. Wang, J. Wicks, Y. Xu, Y. Li, C. M. Gabardo, C.-T. Dinh, Y. Wang, T.-T. Zhuang, D. Sinton and E. H. Sargent, *Nat. Catal.*, 2020, **3**, 75–82.

51 Y. Hori, A. Murata and R. Takahashi, *J. Chem. Soc., Faraday Trans. 1*, 1989, **85**, 2309–2326.

52 W. Tang, A. A. Peterson, A. S. Varela, Z. P. Jovanov, L. Bech, W. J. Durand, S. Dahl, J. K. Nørskov and I. Chorkendorff, *Phys. Chem. Chem. Phys.*, 2012, **14**, 76–81.

53 M. Gonçalves, A. Gomes, J. Condeço, R. Fernandes, T. Pardal, C. Sequeira and J. Branco, *Energy Convers. Manage.*, 2010, **51**, 30–32.

54 M. Goncalves, A. Gomes, J. Condeço, T. Fernandes, T. Pardal, C. Sequeira and J. Branco, *Electrochim. Acta*, 2013, **102**, 388–392.

55 S. Sen, D. Liu and G. T. R. Palmore, *ACS Catal.*, 2014, **4**, 3091–3095.

56 R. Reske, H. Mistry, F. Behafarid, B. Roldan Cuenya and P. Strasser, *J. Am. Chem. Soc.*, 2014, **136**, 6978–6986.

57 J.-F. Xie, Y.-X. Huang, W.-W. Li, X.-N. Song, L. Xiong and H.-Q. Yu, *Electrochim. Acta*, 2014, **139**, 137–144.

58 A. Loiudice, P. Lobaccaro, E. A. Kamali, T. Thao, B. H. Huang, J. W. Ager and R. Buonsanti, *Angew. Chem., Int. Ed.*, 2016, **55**, 5789–5792.

59 M. S. Xie, B. Y. Xia, Y. Li, Y. Yan, Y. Yang, Q. Sun, S. H. Chan, A. Fisher and X. Wang, *Energy Environ. Sci.*, 2016, **9**, 1687–1695.

60 H. Song, M. Im, J. T. Song, J.-A. Lim, B.-S. Kim, Y. Kwon, S. Ryu and J. Oh, *Appl. Catal., B*, 2018, **232**, 391–396.

61 F. Scholten, I. Sinev, M. Bernal and B. Roldan Cuenya, *ACS Catal.*, 2019, **9**, 5496–5502.

62 R. Kas, R. Kortlever, A. Milbrat, M. T. Koper, G. Mul and J. Baltrusaitis, *Phys. Chem. Chem. Phys.*, 2014, **16**, 12194–12201.

63 D. Kim, S. Lee, J. D. Ocon, B. Jeong, J. K. Lee and J. Lee, *Phys. Chem. Chem. Phys.*, 2015, **17**, 824–830.

64 D. Ren, Y. Deng, A. D. Handoko, C. S. Chen, S. Malkhandi and B. S. Yeo, *ACS Catal.*, 2015, **5**, 2814–2821.

65 C.-T. Dinh, T. Burdyny, M. G. Kibria, A. Seifitokaldani, C. M. Gabardo, F. P. García de Arquer, A. Kiani, J. P. Edwards, P. De Luna, O. S. Bushuyev, C. Zou, R. Quintero-Bermudez, Y. Pang, D. Sinton and E. H. Sargent, *Science*, 2018, **360**, 783–787.

66 S. Ma, M. Sadakiyo, R. Luo, M. Heima, M. Yamauchi and P. J. A. Kenis, *J. Power Sources*, 2016, **301**, 219–228.

67 J. Gao, D. Ren, X. Guo, S. M. Zakeeruddin and M. Grätzel, *Faraday Discuss.*, 2019, **215**, 282–296.

68 S. Lee, G. Park and J. Lee, *ACS Catal.*, 2017, **7**, 8594–8604.

69 E. L. Clark, C. Hahn, T. F. Jaramillo and A. T. Bell, *J. Am. Chem. Soc.*, 2017, **139**, 15848–15857.

70 X. Chen, D. A. Henckel, U. O. Nwabara, Y. Li, A. I. Frenkel, T. T. Fister, P. J. Kenis and A. A. Gewirth, *ACS Catal.*, 2019, **10**, 672–682.

71 Y. C. Li, Z. Wang, T. Yuan, D.-H. Nam, M. Luo, J. Wicks, B. Chen, J. Li, F. Li and F. P. G. de Arquer, *J. Am. Chem. Soc.*, 2019, **141**, 8584–8591.

72 Y. Song, R. Peng, D. K. Hensley, P. V. Bonnesen, L. Liang, Z. Wu, H. M. Meyer III, M. Chi, C. Ma and B. G. Sumpter, *ChemistrySelect*, 2016, **1**, 6055–6061.

73 Q. Li, W. Zhu, J. Fu, H. Zhang, G. Wu and S. Sun, *Nano Energy*, 2016, **24**, 1–9.

74 D. Karapinar, N. T. Huan, N. Ranjbar Sahraie, J. Li, D. Wakerley, N. Touati, S. Zanna, D. Taverna, L. H. Galvão Tizei and A. Zitolo, *Angew. Chem., Int. Ed.*, 2019, **58**, 15098–15103.

75 Z. Han, R. Kortlever, H.-Y. Chen, J. C. Peters and T. Agapie, *ACS Cent. Sci.*, 2017, **3**, 853–859.

76 Y. Liu, S. Chen, X. Quan and H. Yu, *J. Am. Chem. Soc.*, 2015, **137**, 11631–11636.

77 Y. Song, S. Wang, W. Chen, S. Li, G. Feng, W. Wei and Y. Sun, *ChemSusChem*, 2019, 293–297.

78 G. Lu, H. Wang, Z. Bian and X. Liu, *Sci. World J.*, 2013, **2013**, 8.

79 C. Xiao and J. Zhang, *ACS Nano*, 2021, **15**, 7975–8000.

80 Z. Chen, T. Wang, B. Liu, D. Cheng, C. Hu, G. Zhang, W. Zhu, H. Wang, Z.-J. Zhao and J. Gong, *J. Am. Chem. Soc.*, 2020, **142**, 6878–6883.

81 M. Wang, Q. Zhang, Q. Xie, L. Wan, Y. Zhao, X. Zhang and J. Luo, *Nanoscale*, 2020, **12**, 17013–17019.

82 W. Fu, Z. Liu, T. Wang, J. Liang, S. Duan, L. Xie, J. Han and Q. Li, *ACS Sustainable Chem. Eng.*, 2020, **8**, 15223–15229.

83 Z. Tan, T. Peng, X. Tan, W. Wang, X. Wang, Z. Yang, H. Ning, Q. Zhao and M. Wu, *ChemElectroChem*, 2020, **7**, 2020–2025.

84 B. Liu, C. Cai, B. Yang, K. Chen, Y. Long, Q. Wang, S. Wang, G. Chen, H. Li, J. Hu, J. Fu and M. Liu, *Electrochim. Acta*, 2021, **388**, 138552.

85 K. Jiang, Y. Huang, G. Zeng, F. M. Toma, W. A. Goddard and A. T. Bell, *ACS Energy Lett.*, 2020, **5**, 1206–1214.

86 Y. Chen, C. W. Li and M. W. Kanan, *J. Am. Chem. Soc.*, 2012, **134**, 19969–19972.

87 S. Wang, T. Kou, S. E. Baker, E. B. Duoss and Y. Li, *Mater. Today Nano*, 2020, **12**, 100096.

88 C. Chen, X. Yan, Y. Wu, S. Liu, X. Sun, Q. Zhu, R. Feng, T. Wu, Q. Qian, H. Liu, L. Zheng, J. Zhang and B. Han, *Chem. Sci.*, 2021, **12**, 5938–5943.

89 F. Yang, P. Deng, Q. Wang, J. Zhu, Y. Yan, L. Zhou, K. Qi, H. Liu, H. S. Park and B. Y. Xia, *J. Mater. Chem. A*, 2020, **8**, 12418–12423.

90 D. Cheng, Z.-J. Zhao, G. Zhang, P. Yang, L. Li, H. Gao, S. Liu, X. Chang, S. Chen, T. Wang, G. A. Ozin, Z. Liu and J. Gong, *Nat. Commun.*, 2021, **12**, 395.

91 F. Dattila, R. García-Muelas and N. López, *ACS Energy Lett.*, 2020, **5**, 3176–3184.

92 P. Qi, L. Zhao, Z. Deng, H. Sun, H. Li, Q. Liu, X. Li, Y. Lian, J. Cheng, J. Guo, Y. Cui and Y. Peng, *J. Phys. Chem. Lett.*, 2021, **12**, 3941–3950.

93 Y.-J. Zhang and A. A. Peterson, *Phys. Chem. Chem. Phys.*, 2015, **17**, 4505–4515.

94 C.-C. Chang, E. Y. Li and M.-K. Tsai, *Phys. Chem. Chem. Phys.*, 2018, **20**, 16906–16909.

95 P. Sirkiä, T. Saario, K. Maekelae, T. Laitinen and M. Bojinov, *Electric and Electrochemical Properties of Surface Films Formed on Copper in the Presence of Bicarbonate Anions, Radiation and Nuclear Safety Authority*, 1999.

96 Y. Hori, H. Konishi, T. Futamura, A. Murata, O. Koga, H. Sakurai and K. Oguma, *Electrochim. Acta*, 2005, **50**, 5354–5369.

97 L. Mandal, K. R. Yang, M. R. Motapothula, D. Ren, P. Lobaccaro, A. Patra, M. Sherburne, V. S. Batista, B. S. Yeo and J. W. Ager, *ACS Appl. Mater. Interfaces*, 2018, **10**, 8574–8584.

98 Q. Lei, H. Zhu, K. Song, N. Wei, L. Liu, D. Zhang, J. Yin, X. Dong, K. Yao, N. Wang, X. Li, B. Davaasuren, J. Wang and Y. Han, *J. Am. Chem. Soc.*, 2020, **142**, 4213–4222.

99 Y. Lum and J. W. Ager, *Angew. Chem., Int. Ed.*, 2018, **57**, 551–554.

100 A. Eilert, F. Cavalca, F. S. Roberts, J. r. Osterwalder, C. Liu, M. Favaro, E. J. Crumlin, H. Ogasawara, D. Friebel and L. G. Pettersson, *J. Phys. Chem. Lett.*, 2016, **8**, 285–290.

101 C. Liu, M. P. Lourenço, S. Hedström, F. Cavalca, O. Diaz-Morales, H. A. Duarte, A. Nilsson and L. G. Pettersson, *J. Phys. Chem. C*, 2017, **121**, 25010–25017.

102 H. Xiang, S. Rasul, K. Scott, J. Portoles, P. Cumpson and H. Y. Eileen, *J. CO₂ Util.*, 2019, **30**, 214–221.

103 M. Watanabe, M. Shibata, A. Kato, M. Azuma and T. Sakata, *J. Electrochem. Soc.*, 1991, **138**, 3382–3389.

104 P. Hirunsit, *J. Phys. Chem. C*, 2013, **117**, 8262–8268.

105 A. Dutta, I. Z. Montiel, R. Erni, K. Kiran, M. Rahaman, J. Drnec and P. Broekmann, *Nano Energy*, 2020, **68**, 104331.

106 L. R. L. Ting, O. Piqué, S. Y. Lim, M. Tanhaei, F. Calle-Vallejo and B. S. Yeo, *ACS Catal.*, 2020, **10**, 4059–4069.

107 X.-G. Zhang, S. Feng, C. Zhan, D.-Y. Wu, Y. Zhao and Z.-Q. Tian, *J. Phys. Chem. Lett.*, 2020, **11**, 6593–6599.

108 C. G. Morales-Guio, E. R. Cave, S. A. Nitopi, J. T. Feaster, L. Wang, K. P. Kuhl, A. Jackson, N. C. Johnson, D. N. Abram, T. Hatsukade, C. Hahn and T. F. Jaramillo, *Nat. Catal.*, 2018, **1**, 764–771.

109 S. Shen, X. Peng, L. Song, Y. Qiu, C. Li, L. Zhuo, J. He, J. Ren, X. Liu and J. Luo, *Small*, 2019, **15**, 1902229.

110 W. Zhu, K. Zhao, S. Liu, M. Liu, F. Peng, P. An, B. Qin, H. Zhou, H. Li and Z. He, *J. Energy Chem.*, 2019, **37**, 176–182.

111 S. Nellaiappan, N. K. Katiyar, R. Kumar, A. Parui, K. D. Malviya, K. G. Pradeep, A. K. Singh, S. Sharma, C. S. Tiwary and K. Biswas, *ACS Catal.*, 2020, **10**, 3658–3663.

112 A. N. Kuhn, H. Zhao, U. O. Nwabara, X. Lu, M. Liu, Y.-T. Pan, W. Zhu, P. J. A. Kenis and H. Yang, *Adv. Funct. Mater.*, 2021, **31**, 2101668.

113 A. Herzog, A. Bergmann, H. S. Jeon, J. Timoshenko, S. Kühl, C. Rettenmaier, M. Lopez Luna, F. T. Haase and B. Roldan Cuenya, *Angew. Chem., Int. Ed.*, 2021, **60**, 7426–7435.

114 X. Zhang, J. Li, Y.-Y. Li, Y. Jung, Y. Kuang, G. Zhu, Y. Liang and H. Dai, *J. Am. Chem. Soc.*, 2021, **143**, 3245–3255.

115 S. Dongare, N. Singh, H. Bhunia and P. K. Bajpai, *Electrochim. Acta*, 2021, **392**, 138988.

116 Z. Li, R. M. Yadav, L. Sun, T. Zhang, J. Zhang, P. M. Ajayan and J. Wu, *Appl. Catal., A*, 2020, **606**, 117829.

117 X. Su, Y. Sun, L. Jin, L. Zhang, Y. Yang, P. Kerns, B. Liu, S. Li and J. He, *Appl. Catal., B*, 2020, **269**, 118800.

118 Y. Song, J. R. C. Junqueira, N. Sikdar, D. Öhl, S. Dieckhöfer, T. Quast, S. Seisel, J. Masa, C. Andronescu and W. Schuhmann, *Angew. Chem., Int. Ed.*, 2021, **60**, 9135–9141.

119 A. H. M. da Silva, S. J. Raaijman, C. S. Santana, J. M. Assaf, J. F. Gomes and M. T. M. Koper, *J. Electroanal. Chem.*, 2021, **880**, 114750.

120 D. Karapinar, C. E. Creissen, J. G. Rivera de la Cruz, M. W. Schreiber and M. Fontecave, *ACS Energy Lett.*, 2021, **6**, 694–706.

121 Y. Feng, Z. Li, H. Liu, C. Dong, J. Wang, S. A. Kulinich and X. Du, *Langmuir*, 2018, **34**, 13544–13549.

122 T.-T. Zhuang, Z.-Q. Liang, A. Seifitokaldani, Y. Li, P. De Luna, T. Burdyny, F. Che, F. Meng, Y. Min and R. Quintero-Bermudez, *Nat. Catal.*, 2018, **1**, 421.

123 Q. Wan, J. Zhang, B. Zhang, D. Tan, L. Yao, L. Zheng, F. Zhang, L. Liu, X. Cheng and B. Han, *Green Chem.*, 2020, **22**, 2750–2754.

124 K. Lv, Y. Fan, Y. Zhu, Y. Yuan, J. Wang, Y. Zhu and Q. Zhang, *J. Mater. Chem. A*, 2018, **6**, 5025–5031.

125 Q. Zhang, S. Tao, J. Du, A. He, Y. Yang and C. Tao, *J. Mater. Chem. A*, 2020, **8**, 8410–8420.

126 L. Ji, L. Li, X. Ji, Y. Zhang, S. Mou, T. Wu, Q. Liu, B. Li, X. Zhu, Y. Luo, X. Shi, A. M. Asiri and X. Sun, *Angew. Chem., Int. Ed.*, 2020, **59**, 758–762.

127 R. Kortlever, I. Peters, C. Balemans, R. Kas, Y. Kwon, G. Mul and M. Koper, *Chem. Commun.*, 2016, **52**, 10229–10232.

128 C. Costentin, M. Robert and J.-M. Savéant, *Chem. Soc. Rev.*, 2013, **42**, 2423–2436.

129 I. Azcarate, C. Costentin, M. Robert and J.-M. Savéant, *J. Am. Chem. Soc.*, 2016, **138**, 16639–16644.

130 H. Takeda, C. Cometto, O. Ishitani and M. Robert, *ACS Catal.*, 2017, **7**, 70–88.

131 J. Qiao, Y. Liu, F. Hong and J. Zhang, *Chem. Soc. Rev.*, 2014, **43**, 631–675.

132 E. Boutin and M. Robert, *Trends Chem.*, 2021, **3**, 359–372.

133 J. Yu, J. Wang, Y. Ma, J. Zhou, Y. Wang, P. Lu, J. Yin, R. Ye, Z. Zhu and Z. Fan, *Adv. Funct. Mater.*, 2021, **1–28**, 2102151.

134 K. Tanaka, Y. Kushi, K. Tsuge, K. Toyohara, T. Nishioka and K. Isobe, *Inorg. Chem.*, 1998, **37**, 120–126.

135 R. Angamuthu, P. Byers, M. Lutz, A. L. Spek and E. Bouwman, *Science*, 2010, **327**, 313–315.

136 M. Meser Ali, H. Sato, T. Mizukawa, K. Tsuge, M.-a. Haga and K. Tanaka, *Chem. Commun.*, 1998, 249–250.

137 H. Nagao, T. Mizukawa and K. Tanaka, *Inorg. Chem.*, 1994, **33**, 3415–3420.

138 K. Toyohara, H. Nagao, T. Mizukawa and K. Tanaka, *Inorg. Chem.*, 1995, **34**, 5399–5400.

139 T. Mizukawa, K. Tsuge, H. Nakajima and K. Tanaka, *Angew. Chem., Int. Ed.*, 1999, **38**, 362–363.

140 H. Nakajima, Y. Kushi, H. Nagao and K. Tanaka, *Organometallics*, 1995, **14**, 5093–5098.

141 K. Tanaka and D. Ooyama, *Coord. Chem. Rev.*, 2002, **226**, 211–218.

142 K. Tanaka and T. Mizukawa, *Appl. Organomet. Chem.*, 2000, **14**, 863–866.

143 G. Neri, I. M. Aldous, J. J. Walsh, L. J. Hardwick and A. J. Cowan, *Chem. Sci.*, 2016, **7**, 1521–1526.

144 T. V. Magdesieva, T. Yamamoto, D. A. Tryk and A. Fujishima, *J. Electrochem. Soc.*, 2002, **149**, D89.

145 N. Sonoyama, M. Kirii and T. Sakata, *Electrochem. Commun.*, 1999, **1**, 213–216.

146 K. Ogura, K. Mine, J. Yano and H. Sugihara, *J. Chem. Soc., Chem. Commun.*, 1993, 20–21.

147 K. Ogura, M. Higasa, J. Yano and N. Endo, *J. Electroanal. Chem.*, 1994, **379**, 373–377.

148 K. Ogura, N. Endo, M. Nakayama and H. Ootsuka, *J. Electrochem. Soc.*, 1995, **142**, 4026–4032.

149 K. Ogura, M. Nakayama and C. Kusumoto, *J. Electrochem. Soc.*, 1996, **143**, 3606–3615.

150 Z. Weng, J. Jiang, Y. Wu, Z. Wu, X. Guo, K. L. Materna, W. Liu, V. S. Batista, G. W. Brudvig and H. Wang, *J. Am. Chem. Soc.*, 2016, **138**, 8076–8079.

151 Z. Weng, Y. Wu, M. Wang, J. Jiang, K. Yang, S. Huo, X. F. Wang, Q. Ma, G. W. Brudvig, V. S. Batista, Y. Liang, Z. Feng and H. Wang, *Nat. Commun.*, 2018, **9**, 1–9.

152 M. Balamurugan, H. Y. Jeong, V. S. K. Choutipalli, J. S. Hong, H. Seo, N. Saravanan, J. H. Jang, K. G. Lee, Y. H. Lee, S. W. Im, V. Subramanian, S. H. Kim and K. T. Nam, *Small*, 2020, **16**, 1–10.

153 N. Sakamoto, Y. F. Nishimura, T. Nonaka, M. Ohashi, N. Ishida, K. Kitazumi, Y. Kato, K. Sekizawa, T. Morikawa and T. Arai, *ACS Catal.*, 2020, **10**, 10412–10419.

154 J. X. Wu, S. Z. Hou, X. D. Zhang, M. Xu, H. F. Yang, P. S. Cao and Z. Y. Gu, *Chem. Sci.*, 2019, **10**, 2199–2205.

155 F. Yang, A. Chen, P. L. Deng, Y. Zhou, Z. Shahid, H. Liu and B. Y. Xia, *Chem. Sci.*, 2019, **10**, 7975–7981.

156 D. Karapinar, N. T. Huan, N. Ranjbar Sahraie, J. Li, D. Wakerley, N. Touati, S. Zanna, D. Taverna, L. H. Galvão Tizei, A. Zitolo, F. Jaouen, V. Mougel and M. Fontecave, *Angew. Chem., Int. Ed.*, 2019, **58**, 15098–15103.

157 Y. Song, R. Peng, D. K. Hensley, P. V. Bonnesen, L. Liang, Z. Wu, H. M. Meyer, M. Chi, C. Ma, B. G. Sumpter and A. J. Rondinone, *ChemistrySelect*, 2016, **1**, 6055–6061.

158 M. Hammouche, D. Lexa and J. M. Saveant, *J. Electroanal. Chem.*, 1988, **249**, 347–351.

159 A. Thevenon, A. Rosas-Hernández, J. C. Peters and T. Agapie, *Angew. Chem., Int. Ed.*, 2019, **58**, 16952–16958.

160 X. Wang, Z. Wang, F. P. García de Arquer, C. T. Dinh, A. Ozden, Y. C. Li, D. H. Nam, J. Li, Y. S. Liu, J. Wicks, Z. Chen, M. Chi, B. Chen, Y. Wang, J. Tam, J. Y. Howe, A. Proppe, P. Todorović, F. Li, T. T. Zhuang, C. M. Gabardo, A. R. Kirmani, C. McCallum, S. F. Hung, Y. Lum, M. Luo, Y. Min, A. Xu, C. P. O'Brien, B. Stephen, B. Sun, A. H. Ip, L. J. Richter, S. O. Kelley, D. Sinton and E. H. Sargent, *Nat. Energy*, 2020, **5**, 478–486.

161 W. A. Thompson, E. Sanchez Fernandez and M. M. Maroto-Valer, *ACS Sustainable Chem. Eng.*, 2020, **8**, 4677–4692.

162 E. M. Cedeño Morales, B. I. Kharisov and M. A. Méndez-Rojas, *Mater. Today: Proc.*, 2021, **46**, 2982–2997.

163 Y. Zhang, B. Xia, J. Ran, K. Davey and S. Z. Qiao, *Adv. Energy Mater.*, 2020, **10**, 1903879.

164 S. Matavos-Aramyan, S. Soukhakian, M. H. Jazebizadeh, M. Moussavi and M. R. Hojjati, *Appl. Mater. Today*, 2020, **18**, 100499.

165 J. Wang, S. Lin, N. Tian, T. Ma, Y. Zhang and H. Huang, *Adv. Funct. Mater.*, 2021, **31**, 2008008.

166 X. Jiao, K. Zheng, L. Liang, X. Li, Y. Sun and Y. Xie, *Chem. Soc. Rev.*, 2020, **49**, 6592–6604.

167 T. J. LaTempa, S. Rani, N. Bao and C. A. Grimes, *Nanoscale*, 2012, **4**, 2245–2250.

168 C. Wang, R. L. Thompson, P. Ohodnicki, J. Baltrus and C. Matranga, *J. Mater. Chem.*, 2011, **21**, 13452–13457.

169 X. Zhang, F. Han, B. Shi, S. Farsinezhad, G. P. Dechaine and K. Shankar, *Angew. Chem., Int. Ed.*, 2012, **51**, 12732–12735.

170 M. Sayed, L. Zhang and J. Yu, *Chem. Eng. J.*, 2020, **397**, 125390.

171 A. E. Nogueira, G. T. S. T. da Silva, J. A. Oliveira, J. A. Torres, M. G. S. da Silva, M. Carmo and C. Ribeiro, *Catal. Commun.*, 2020, **137**, 105929.

172 J. Zhou, Y. Li, L. Yu, Z. Li, D. Xie, Y. Zhao and Y. Yu, *Chem. Eng. J.*, 2020, **385**, 123940.

173 D. Giusi, C. Ampelli, C. Genovese, S. Perathoner and G. Centi, *Chem. Eng. J.*, 2021, **408**, 127250.

174 C. An, J. Yuan and J. Zhu, *J. Electrochem. Soc.*, 2018, **165**, H1066–H1071.

175 H. Homayoni, W. Chanmanee, N. R. de Tacconi, B. H. Dennis and K. Rajeshwar, *J. Electrochem. Soc.*, 2015, **162**, E115–E122.

176 S. Jiao, X. Fu, L. Zhang, L. Zhang, S. Ruan, Y.-J. Zeng and H. Huang, *Nano Today*, 2021, **36**, 101028.

177 T. Li, X. Dong, W. Chen, X. Zhao, G. Li, G. Feng, Y. Song, W. Wei and Y. Sun, *Appl. Surf. Sci.*, 2020, **526**, 146578.

178 X. Wang, C. Gao, J. Low, K. Mao, D. Duan, S. Chen, R. Ye, Y. Qiu, J. Ma, X. Zheng, R. Long, X. Wu, L. Song, J. Zhu and Y. Xiong, *Sci. Bull.*, 2021, **66**, 1296–1304.

179 X.-D. Zhang, K. Liu, J.-W. Fu, H.-M. Li, H. Pan, J.-H. Hu and M. Liu, *Front. Phys.*, 2021, **16**, 63500.

180 T. Yui, A. Kan, C. Saitoh, K. Koike, T. Ibusuki and O. Ishitani, *ACS Appl. Mater. Interfaces*, 2011, **3**, 2594–2600.

181 Y. Wang, Q. Lai, F. Zhang, X. Shen, M. Fan, Y. He and S. Ren, *RSC Adv.*, 2014, **4**, 44442–44451.

182 S. Yu, A. J. Wilson, J. Heo and P. K. Jain, *Nano Lett.*, 2018, **18**, 2189–2194.

183 K. Hirota, D. A. Tryk, T. Yamamoto, K. Hashimoto, M. Okawa and A. Fujishima, *J. Phys. Chem. B*, 1998, **102**, 9834–9843.

184 K. Zhao, X. W. Nie, H. Z. Wang, S. Chen, X. Quan, H. T. Yu, W. Y. Choi, G. H. Zhang, B. Kim and J. G. G. Chen, *Nat. Commun.*, 2020, **11**, 10.

185 B. Bian, S. Bajracharya, J. J. Xu, D. Pant and P. E. Saikaly, *Bioresour. Technol.*, 2020, **302**, 12.

186 L. Jourdin and T. Burdyny, *Trends Biotechnol.*, 2021, **39**, 359–369.

187 L. Jourdin, S. Freguia, V. Flexer and J. Keller, *Environ. Sci. Technol.*, 2016, **50**, 1982–1989.

188 D. Zang, Q. Li, G. Dai, M. Zeng, Y. Huang and Y. Wei, *Appl. Catal., B*, 2021, **281**, 119426.

189 X. Li, S. Chen, D. Liang and M. Alvarado-Moralesa, *J. Power Sources*, 2020, **477**, 228990.

190 S. Srikanth, D. Singh, K. Vanbroekhoven, D. Pant, M. Kumar, S. K. Puri and S. S. V. Ramakumar, *Bioresour. Technol.*, 2018, **265**, 45–51.

191 Z.-Q. Liang, T.-T. Zhuang, A. Seifitokaldani, J. Li, C.-W. Huang, C.-S. Tan, Y. Li, P. De Luna, C. T. Dinh, Y. Hu, Q. Xiao, P.-L. Hsieh, Y. Wang, F. Li, R. Quintero-Bermudez, Y. Zhou, P. Chen, Y. Pang, S.-C. Lo, L.-J. Chen, H. Tan, Z. Xu, S. Zhao, D. Sinton and E. H. Sargent, *Nat. Commun.*, 2018, **9**, 3828.

192 J. Annie Modestra, R. Katakojwala and S. Venkata Mohan, *Chem. Eng. J.*, 2020, **394**, 124759.

193 S. Bajracharya, S. Srikanth, G. Mohanakrishna, R. Zacharia, D. P. B. T. B. Strik and D. Pant, *J. Power Sources*, 2017, **356**, 256–273.

194 A. G. Fast and E. T. Papoutsakis, *Curr. Opin. Chem. Eng.*, 2012, **1**, 380–395.

195 K. P. Nevin, S. A. Hensley, A. E. Franks, Z. M. Summers, J. H. Ou, T. L. Woodard, O. L. Snoeyenbos-West and D. R. Lovley, *Appl. Environ. Microbiol.*, 2011, **77**, 2882–2886.

196 V. G. Debabov, *Microbiology*, 2021, **90**, 273–297.

197 G. Merli, A. Becci, A. Amato and F. Beolchini, *Sci. Total Environ.*, 2021, **798**, 149292.

198 D. R. Lovley and K. P. Nevin, *Curr. Opin. Biotechnol.*, 2013, **24**, 385–390.

199 B. Bian, S. Bajracharya, J. Xu, D. Pant and P. E. Saikaly, *Bioresour. Technol.*, 2020, **302**, 122863.

200 H.-Y. Yang, N.-N. Hou, Y.-X. Wang, J. Liu, C.-S. He, Y.-R. Wang, W.-H. Li and Y. Mu, *Sci. Total Environ.*, 2021, **790**, 148128.

201 M. Roy, R. Yadav, P. Chiranjeevi and S. A. Patil, *Bioresour. Technol.*, 2021, **320**, 124289.

202 S. Das, S. Das and M. M. Ghangrekar, *Process Biochem.*, 2021, **101**, 237–246.

203 Y. Jiang, Q. Liang, N. Chu, W. Hao, L. Zhang, G. Zhan, D. Li and R. J. Zeng, *Sci. Total Environ.*, 2020, **741**, 140198.

204 P. Izadi, J.-M. Fontmorin, A. Godain, E. H. Yu and I. M. Head, *npj Biofilms Microbiomes*, 2020, **6**, 40.

205 J. Philips, *Front. Microbiol.*, 2020, **10**, 2997.

206 I. Vassilev, P. A. Hernandez, P. Batlle-Vilanova, S. Freguia, J. O. Kromer, J. Keller, P. Ledezma and B. Virdis, *ACS Sustainable Chem. Eng.*, 2018, **6**, 8485–8493.

207 R. Ganigue, P. Sanchez-Paredes, L. Baneras and J. Colprim, *Front. Microbiol.*, 2016, **7**, 702.

208 H. D. May, P. J. Evans and E. V. LaBelle, *Curr. Opin. Biotechnol.*, 2016, **42**, 225–233.

209 J. B. A. Arends, S. A. Patil, H. Roume and K. Rabaey, *J. CO2 Util.*, 2017, **20**, 141–149.

210 E. V. LaBelle, C. W. Marshall, J. A. Gilbert and H. D. May, *PLoS One*, 2014, **9**, e109935.

211 E. Perona-Vico, L. Feliu-Paradeda, S. Puig and L. Bañeras, *Sci. Rep.*, 2020, **10**, 19852.

212 P. Izadi, J.-M. Fontmorin, S. S. Lim, I. Head and E. H. Yu, *Faraday Discuss.*, 2021, **230**, 344–359.

213 A. Prévoteau, J. M. Carvajal-Arroyo, R. Ganigué and K. Rabaey, *Curr. Opin. Biotechnol.*, 2020, **62**, 48–57.

214 F. Aulenta, L. Catapano, L. Snip, M. Villano and M. Majone, *ChemSusChem*, 2012, **5**, 1080–1085.

215 K. W. Meereboer, M. Misra and A. K. Mohanty, *Green Chem.*, 2020, **22**, 5519–5558.

216 F. A. El-malek, H. Khairy, A. Farag and S. Omar, *Int. J. Biol. Macromol.*, 2020, **157**, 319–328.

217 J. Medeiros Garcia Alcântara, F. Distante, G. Storti, D. Moscatelli, M. Morbidelli and M. Sponchioni, *Biotechnol. Adv.*, 2020, **42**, 107582.

218 M. Liu, M. Arshadi, F. Javi, P. Lawrence, S. M. Davachi and A. Abbaspourrad, *J. Cleaner Prod.*, 2020, **276**, 123353.

219 B. Yadav, A. Pandey, L. R. Kumar and R. D. Tyagi, *Bioresour. Technol.*, 2020, **298**, 122584.

220 T. Pepè Sciarria, P. Batlle-Vilanova, B. Colombo, B. Scaglia, M. D. Balaguer, J. Colprim, S. Puig and F. Adani, *Green Chem.*, 2018, **20**, 4058–4066.

221 M. Stöckl, S. Harms, I. Dinges, S. Dimitrova and D. Holtmann, *ChemSusChem*, 2020, **13**, 4086–4093.

222 V. Sivalingam, V. Ahmadi, O. Babafemi and C. Dinamarca, *Catalysts*, 2021, **11**, 40.

223 Z. Gong, H. Yu, J. Zhang, F. Li and H. Song, *Synth. Syst. Biotechnol.*, 2020, **5**, 304–313.

224 Y. Jiang, H. D. May, L. Lu, P. Liang, X. Huang and Z. J. Ren, *Water Res.*, 2019, **149**, 42–55.

225 O. Choi, T. Kim, H. M. Woo and Y. Um, *Sci. Rep.*, 2014, **4**, 6961.

226 S. Zhang, J. Jiang, H. Wang, F. Li, T. Hua and W. Wang, *J. CO2 Util.*, 2021, **51**, 101640.

227 O. Cabau-Peinado, A. J. J. Straathof and L. Jourdin, *Front. Microbiol.*, 2021, **12**, 669218.

228 N. Chu, Q. Liang, W. Zhang, Z. Ge, W. Hao, Y. Jiang and R. J. Zeng, *ACS Sustainable Chem. Eng.*, 2020, **8**, 8773–8782.

229 G. Jabeen and R. Farooq, *J. Biosci.*, 2016, **41**, 367–380.

230 I. Vassilev, F. Kracke, S. Freguia, J. Keller, J. O. Krömer, P. Ledezma and B. Virdis, *Chem. Commun.*, 2019, **55**, 4351–4354.

231 I. Vassilev, P. A. Hernandez, P. Batlle-Vilanova, S. Freguia, J. O. Krömer, J. Keller, P. Ledezma and B. Virdis, *ACS Sustainable Chem. Eng.*, 2018, **6**, 8485–8493.

232 L. Jourdin, S. M. T. Raes, C. J. N. Buisman and D. P. B. T. B. Strik, *Front. Energy Res.*, 2018, **6**, 7.

233 P. L. Tremblay and T. Zhang, *Front. Microbiol.*, 2015, **6**, 201.

234 B. Schiel-Bengelsdorf and P. Durre, *FEBS Lett.*, 2012, **586**, 2191–2198.

235 C. W. Marshall, D. E. Ross, E. B. Fichot, R. S. Norman and H. D. May, *Environ. Sci. Technol.*, 2013, **47**, 6023–6029.

236 P. Batlle-Vilanova, S. Puig, R. Gonzalez-Olmos, M. D. Balaguer and J. Colprim, *J. Chem. Technol. Biotechnol.*, 2016, **91**, 921–927.

237 P. Izadi, J.-M. Fontmorin, B. Virdis, I. M. Head and E. H. Yu, *Appl. Energy*, 2021, **283**, 116310.

238 S. Gildemyn, K. Verbeeck, R. Slabbinck, S. J. Andersen, A. Prevoteau and K. Rabaey, *Environ. Sci. Technol. Lett.*, 2015, **2**, 325–328.

239 L. Jourdin, T. Grieger, J. Monetti, V. Flexer, S. Freguia, Y. Lu, J. Chen, M. Romano, G. G. Wallace and J. Keller, *Environ. Sci. Technol.*, 2015, **49**, 13566–13574.

240 H. Liang, X. Ma, W. Ning, Y. Liu, A. J. Sinskey, G. Stephanopoulos and K. Zhou, *Metab. Eng.*, 2021, **65**, 223–231.

241 F. V. Gambacorta, J. J. Dietrich, Q. Yan and B. F. Pfleger, *Curr. Opin. Chem. Biol.*, 2020, **59**, 182–192.

242 R. Miao, H. Xie, X. Liu, P. Lindberg and P. Lindblad, *Curr. Opin. Chem. Biol.*, 2020, **59**, 69–76.

243 P. N. Ashani, M. Shafiei and K. Karimi, *Bioresour. Technol.*, 2020, **308**, 123267.

244 X. Zhen, Y. Wang and D. Liu, *Renewable Energy*, 2020, **147**, 2494–2521.

245 J. Lee, Y.-S. Jang, S. J. Choi, J. A. Im, H. Song, J. H. Cho, D. Y. Seung, E. T. Papoutsakis, G. N. Bennett and S. Y. Lee, *Appl. Environ. Microbiol.*, 2012, **78**, 1416–1423.

246 S. Y. Lee, Y. S. Jang, J. Y. Lee and J. Lee, *J. Biotechnol.*, 2010, **150**, S557.

247 I. Vassilev, F. Kracke, S. Freguia, J. Keller, J. O. Kromer, P. Ledezma and B. Virdis, *Chem. Commun.*, 2019, **55**, 4351–4354.

248 C. M. Spirito, H. Richter, K. Rabaey, A. J. M. Stams and L. T. Angenent, *Curr. Opin. Biotechnol.*, 2014, **27**, 115–122.

249 C. Delacourt, P. L. Ridgway, J. B. Kerr and J. Newman, *J. Electrochem. Soc.*, 2008, **155**, B42–B49.

250 O. Aschenbrenner and P. Styring, *Energy Environ. Sci.*, 2010, **3**, 1106–1113.

251 F. Proietto, B. Schiavo, A. Galia and O. Scialdone, *Electrochim. Acta*, 2018, **277**, 30–40.

252 Z. M. Yang, D. Li, L. Xing, H. Xiang, J. Xuan, S. A. Cheng, E. H. Yu and A. D. Yang, *ACS Sustainable Chem. Eng.*, 2021, **9**, 351–361.

253 A. Del Castillo, M. Alvarez-Guerra, J. Solla-Gullón, A. Sáez, V. Montiel and A. Irabien, *J. CO₂ Util.*, 2017, **18**, 222–228.

254 P. Jeanty, C. Scherer, E. Magori, K. Wiesner-Fleischer, O. Hinrichsen and M. Fleischer, *J. CO₂ Util.*, 2018, **24**, 454–462.

255 D. Kopljar, A. Inan, P. Vindayer, N. Wagner and E. Klemm, *J. Appl. Electrochem.*, 2014, **44**, 1107–1116.

256 D. Higgins, C. Hahn, C. Xiang, T. F. Jaramillo and A. Z. Weber, *ACS Energy Lett.*, 2019, **4**, 317–324.

257 Y. C. Li, D. Zhou, Z. Yan, R. H. Gonçalves, D. A. Salvatore, C. P. Berlinguette and T. E. Mallouk, *ACS Energy Lett.*, 2016, **1**, 1149–1153.

258 D. A. Vermaas and W. A. Smith, *ACS Energy Lett.*, 2016, **1**, 1143–1148.

259 D. A. Salvatore, D. M. Weekes, J. He, K. E. Dettelbach, Y. C. Li, T. E. Mallouk and C. P. Berlinguette, *ACS Energy Lett.*, 2018, **3**, 149–154.

260 Z. Yan, J. L. Hitt, Z. Zeng, M. A. Hickner and T. E. Mallouk, *Nat. Chem.*, 2021, **13**, 33–40.

261 D. M. Weekes, D. A. Salvatore, A. Reyes, A. Huang and C. P. Berlinguette, *Acc. Chem. Res.*, 2018, **51**, 910–918.

262 J. A. Rabinowitz and M. W. Kanan, *Nat. Commun.*, 2020, **11**, 5231.

263 D. T. Whipple, E. C. Finke and P. J. A. Kenis, *Electrochem. Solid-State Lett.*, 2010, **13**, B109–B111.

264 H. Wang, D. Y. C. Leung and J. Xuan, *Appl. Energy*, 2013, **102**, 1057–1062.

265 E. V. Kondratenko, G. Mul, J. Baltrusaitis, G. O. Larrazábal and J. Pérez-Ramírez, *Energy Environ. Sci.*, 2013, **6**, 3112–3135.

266 G. Kaur, A. P. Kulkarni, S. Giddey and S. P. S. Badwal, *Appl. Energy*, 2018, **221**, 131–138.

267 Y. Tao, S. D. Ebbesen and M. B. Mogensen, *J. Electrochem. Soc.*, 2014, **161**, F337–F343.

268 L. Zhang, S. Hu, X. Zhu and W. Yang, *J. Energy Chem.*, 2017, **26**, 593–601.

269 S. Perathoner and G. Centi, *ChemSusChem*, 2014, **7**, 1274–1282.

270 D. R. Kauffman, J. Thakkar, R. Siva, C. Matranga, P. R. Ohodnicki, C. Zeng and R. Jin, *ACS Appl. Mater. Interfaces*, 2015, **7**, 15626–15632.

271 S. H. Jensen, C. Graves, M. Mogensen, C. Wendel, R. Braun, G. Hughes, Z. Gao and S. A. Barnett, *Energy Environ. Sci.*, 2015, **8**, 2471–2479.

272 X. Li, P. Anderson, H.-R. M. Jhong, M. Paster, J. F. Stubbins and P. J. A. Kenis, *Energy Fuels*, 2016, **30**, 5980–5989.

273 C. Delacourt, P. L. Ridgway and J. Newman, *J. Electrochem. Soc.*, 2010, **157**, B1902.

274 J. Wu, F. G. Risalvato, P. P. Sharma, P. J. Pellechia, F.-S. Ke and X.-D. Zhou, *J. Electrochem. Soc.*, 2013, **160**, F953–F957.

275 O. Scialdone, A. Galia, G. L. Nero, F. Proietto, S. Sabatino and B. Schiavo, *Electrochim. Acta*, 2016, **199**, 332–341.

276 M. A. Méndez, P. Voyame and H. H. Girault, *Angew. Chem., Int. Ed.*, 2011, **50**, 7391–7394.

277 T. Burdyny, P. J. Graham, Y. Pang, C.-T. Dinh, M. Liu, E. H. Sargent and D. Sinton, *ACS Sustainable Chem. Eng.*, 2017, **5**, 4031–4040.

278 Y. Lum, B. Yue, P. Lobaccaro, A. T. Bell and J. W. Ager, *J. Phys. Chem. C*, 2017, **121**, 14191–14203.

279 R. Kas, R. Kortlever, H. Yılmaz, M. T. M. Koper and G. Mul, *ChemElectroChem*, 2015, **2**, 354–358.

280 D. Chu, G. Qin, X. Yuan, M. Xu, P. Zheng and J. Lu, *ChemSusChem*, 2008, **1**, 205–209.

281 S. Kaneco, H. Katsumata, T. Suzuki and K. Ohta, *Energy Fuels*, 2006, **20**, 409–414.

282 E. J. Dufek, T. E. Lister, S. G. Stone and M. E. McIlwain, *J. Electrochem. Soc.*, 2012, **159**, F514–F517.

283 N. Gutiérrez-Guerra, L. Moreno-López, J. C. Serrano-Ruiz, J. L. Valverde and A. de Lucas-Consuegra, *Appl. Catal., B*, 2016, **188**, 272–282.

284 R. D. Rogers and K. R. Seddon, *Science*, 2003, **302**, 792–793.

285 J. F. Brennecke and B. E. Gurkan, *J. Phys. Chem. Lett.*, 2010, **1**, 3459–3464.

286 S. F. R. Taylor, C. McCrellis, C. McStay, J. Jacquemin, C. Hardacre, M. Mercy, R. G. Bell and N. H. de Leeuw, *J. Solution Chem.*, 2015, **44**, 511–527.

287 N. Hollingsworth, S. F. R. Taylor, M. T. Galante, J. Jacquemin, C. Longo, K. B. Holt, N. H. de Leeuw and C. Hardacre, *Angew. Chem., Int. Ed.*, 2015, **54**, 14164–14168.

288 Y. Chen and T. Mu, *Green Chem.*, 2019, **21**, 2544–2574.

289 X. Sun, Q. Zhu, X. Kang, H. Liu, Q. Qian, J. Ma, Z. Zhang, G. Yang and B. Han, *Green Chem.*, 2017, **19**, 2086–2091.

290 H. Ning, W. Wang, Q. H. Mao, S. R. Zheng, Z. X. Yang, Q. S. Zhao and M. B. Wu, *Acta Phys.-Chim. Sin.*, 2018, **34**, 938–944.

291 R. F. Zarandi, B. Rezaei, H. S. Ghaziaskar and A. A. Ensafi, *J. Environ. Chem. Eng.*, 2019, **7**, 103141.

292 H. Xiao, T. Cheng, W. A. Goddard and R. Sundararaman, *J. Am. Chem. Soc.*, 2016, **138**, 483–486.

293 T. Cheng, H. Xiao and W. A. Goddard, *J. Phys. Chem. Lett.*, 2015, **6**, 4767–4773.

294 Z. J. Zhao, S. H. Liu, S. J. Zha, D. F. Cheng, F. Studt, G. Henkelman and J. L. Gong, *Nat. Rev. Mater.*, 2019, **4**, 792–804.

295 F. Studt, *Front. Catal.*, 2021, **1**, 658965.

296 A. A. Latimer, A. R. Kulkarni, H. Aljama, J. H. Montoya, J. S. Yoo, C. Tsai, F. Abild-Pedersen, F. Studt and J. K. Nørskov, *Nat. Mater.*, 2017, **16**, 225–229.

297 X. Zhang, J. X. Liu, B. Zijlstra, I. A. W. Filot, Z. Y. Zhou, S. G. Sun and E. J. M. Hensen, *Nano Energy*, 2018, **43**, 200–209.

298 L. Lin, H. B. Li, C. C. Yan, H. F. Li, R. Si, M. R. Li, J. P. Xiao, G. X. Wang and X. H. Bao, *Adv. Mater.*, 2019, **31**, 7.

299 Y. F. Song, W. Chen, C. C. Zhao, S. G. Li, W. Wei and Y. H. Sun, *Angew. Chem., Int. Ed.*, 2017, **56**, 10840–10844.

300 R. Zhang, G. Wang, B. Wang and L. Ling, *J. Phys. Chem. C*, 2014, **118**, 5243–5254.

301 I. M. B. Nielsen and K. Leung, *J. Phys. Chem. A*, 2010, **114**, 10166–10173.

302 K. Leung, I. M. B. Nielsen, N. Sai, C. Medforth and J. A. Shelnutt, *J. Phys. Chem. A*, 2010, **114**, 10174–10184.

303 L. I. Bendavid and E. A. Carter, *J. Phys. Chem. C*, 2013, **117**, 26048–26059.

304 Q.-J. Hong and Z.-P. Liu, *Surf. Sci.*, 2010, **604**, 1869–1876.

305 J.-S. Filhol and M. Neurock, *Angew. Chem., Int. Ed.*, 2006, **45**, 402–406.

306 Y. Zheng, A. Vasileff, X. Zhou, Y. Jiao, M. Jaroniec and S.-Z. Qiao, *J. Am. Chem. Soc.*, 2019, **141**, 7646–7659.

307 H. Zhang, H. Wang, K. Jiao and J. Xuan, *Appl. Energy*, 2020, **268**, 115053.

308 J.-M. Fontmorin, P. Izadi, D. Li, S. S. Lim, S. Farooq, S. S. Bilal, S. A. Cheng and E. H. Yu, *Electrochim. Acta*, 2021, **372**, 137853.